CHALMERS
UNIVERSITY OF TECHNOLOGY

A study of electrolytes for rechargeable zinc-metal batteries

Master's thesis in Physics

ALEXANDER ENGBLOM

DEPARTMENT OF PHYSICS

Chalmers University of Technology

Gothenburg, Sweden 2022

www.chalmers.se

Master's thesis 2022

A study of electrolytes for rechargeable zinc-metal batteries

ALEXANDER ENGBLOM

CHALMERS
UNIVERSITY OF TECHNOLOGY

Department of Physics
Division of Material Physics
Chalmers University of Technology
Gothenburg, Sweden 2022

A study of electrolytes for rechargeable zinc-metal batteries

ALEXANDER ENGBLOM

Supervisor: Shizhao Xiong, Division of Material Physics
Examiner: Aleksandar Matic, Division of Material Physics

Master's Thesis 2022
Department of Physics
Division of Material Physics
Chalmers University of Technology
SE-412 96 Gothenburg
Telephone +46 31 772 1000

Abstract

Today batteries can be found in a large variety of products and the use of batteries increases every year. However, current battery technologies are approaching their limit and will likely struggle to keep up with future demands. Due to this, battery technology must take a leap forward and explore new chemistries and concepts. One promising candidate for this is the zinc-metal battery, which is made out of more environmentally friendly and safer materials and could offer high energy density. However, the disadvantage of zinc-metal batteries is their short cycle life which is caused by the growth of zinc dendrites, inducing short circuiting. There have been several approaches to suppress the growth of zinc dendrites and electrolyte design is one of the most promising approaches.

In this project electrolyte design, including salt concentration and exploration of additives, was studied with the aim to stabilize the zinc anode in a zinc-metal battery. The salt chosen was zinc sulfate heptahydrate, which was added at different concentration to water to create aqueous electrolytes. Their physical properties such as ion conductivity, viscosity, density, and their infrared and Raman spectrum were then measured. The effect of salt concentration on the stability and Coulombic efficiency of coin cells were also investigated. To explore the effects of additives sulfated cellulose nanocrystals (CNC) and sodium carboxymethyl cellulose (CMC) were added to the electrolyte and the characterization was performed once again on these new electrolytes. How the salt concentration and the additives affected the zinc deposition was studied through the use of scanning electron microscopy (SEM).

The results of this project show that a molar ratio of water and zinc ions between 25:1-50:1 is the most suitable for the stability and Coulombic efficiency of coin cells. The additives did not affect the physical properties of the electrolyte notably, apart from the viscosity. However, they did affect the electrochemical performance, CNC improved the Coulombic efficiency and CMC improved the stability. The SEM images showed that the salt concentration and the additives do affect the morphology of the deposited zinc.

Acknowledgements

Firstly I would like to thank Aleksandar Matic, who has acted as my examiner and been guiding me throughout my work on this project. He always created a good and welcoming environment during our meetings and discussions with his genuine interest in my progress.

I would also want to thank my supervisor Shizhao Xiong, who always was able to answer any questions I had and help me to keep the project moving forward and keep to the deadlines.

Lastly, I am also grateful to everyone at the MF division for giving me a warm welcome and for all of our nice lunches and fikas we have had during my time here in the division.

Contents

1

Introduction

Batteries are taking up an important part of our life in modern society. From the large scale of electrical grid storage to the small scale of our personal devices, batteries play a vital role. The demand for batteries is constantly increasing and this trend is not predicted to change in the near future. This is connected to the rise of renewable energy and increasing use of electronic devices. However, it is worth noting that the biggest part of the increasing demand of energy storage is related to the transportation sector, with the rise of electric vehicles [1]. For most of these applications is it preferential to use rechargeable batteries to lessen the waste produced. When it comes the rechargeable batteries the most widely used type is the lithium ion battery. Lithium ion batteries have high energy density, long cycle life, and have seen a continuous decline in production cost [2].

But lithium ion batteries are not free of flaws. They are expensive, even with the historical decline in price [2]. They also have a high social and environmental cost as well as pose a safety hazard due to the flammability of the liquid electrolyte used [3, 4]. It is also predicted that the supply of the raw materials will not be able to keep up with future demands [5]. All these factors provide a strong driving force to find alternative energy storage technologies. One promising candidate is the zinc-metal battery which is based on more abundant, cheaper, and non-toxic materials compared to lithium ion batteries. Also zinc-metal batteries have a higher theoretical specific capacity [6, 7].

However, zinc-metal batteries are facing their own challenges. The main issue is the rechargeability and thus they have a shorter cycle life than that of lithium ion batteries. This is caused by the zinc anode which is highly preferential to form dendrites during charging. The zinc dendrites will eventually pierce through the separator and induce short circuit of the battery [7]. Many approaches have been developed to prevent the formation of zinc dendrites, including interfacial metal oxide layers, epitaxial electrodeposition, and reducing the water activity at the surface [7–9].

1.1 Aim of project

This project aims to design an electrolyte that can supress the growth of zinc dendrites in a rechargeable zinc-metal battery. More specifically, to study how the components of the electrolyte affect the dendrite growth as well as the electrochemical behavior of the zinc anode. This project focuses on investigating the effects of the salt concentration (zinc sulfate heptahydrate) and additives in an aqueous electrolyte. Sulfated cellulose nanocrystals (CNC) and sodium carboxymethyl cellulose (CMC) are chosen as the additives. This study is conducted by physical characterization of the electrolytes, galvanostatic measurements on symmetric zinc cells and zinc copper cells, and observing the morphology of metal deposition on the electrodes by scanning electron microscopy.

2

Fundamentals of battery

The working principle for a rechargeable battery is outputting usable energy by spontaneous reactions on the anode and the cathode, and also storing energy by reversing the process. The electrochemical reactions can be understood by thermodynamics. For every reaction, there must be a driving force and in a battery, this driving force is the potential between the electrodes [10]. The total energy in the battery is given by Gibbs free energy

$$\Delta G = -nFE_{cell} \tag{2.1}$$

where n is the number of electrons transferred per mole reactant, F is the Faraday constant, and E_{cell} is the equilibrium potential. The reactions taking place in a battery, if assumed to be reversible, can be expressed as

$$O + ne^- \rightleftharpoons R \tag{2.2}$$

where O is the oxidized species and R is the reduced species. To get the potential between the electrodes one can use the Nernst equation[10]

$$E = E^0 + \frac{2.3RT}{nF} log\left(\frac{c_O}{c_R}\right) \tag{2.3}$$

where c_O is the concentration of the oxidized species, c_R is the concentration of the reduced species, T is the temperature and E^0 is the standard potential of the O/R couple. By using this equation for each of the electrodes the equilibrium potential can be obtained. At equilibrium, the rates for reduction of O to R and oxidation of R to O are the same. However, for the equality of equation 2.3 to hold the ratio c_O/c_R will change when a potential is applied. Due to the reactions occurring from this ratio change, there will also be a flow of electrons [10]. This flow of electrons under the potential is the energy that can either be taken out of or stored in the battery.

A battery has several different components that work together to enable the electrochemical reactions. Firstly a battery has two electrodes, the anode and the cathode, which it passes ions between. There are several different types of electrode material that work by different principles, and some examples will be discussed in sections 2.1 and 3. To enable the ion transfer there is an ion conducting electrolyte between the electrodes, as well as a separator. The function of the separator is to create a physical barrier between the electrodes in order to avoid

short circuiting of the battery. A representation of these components in a battery is shown in figure 2.1.

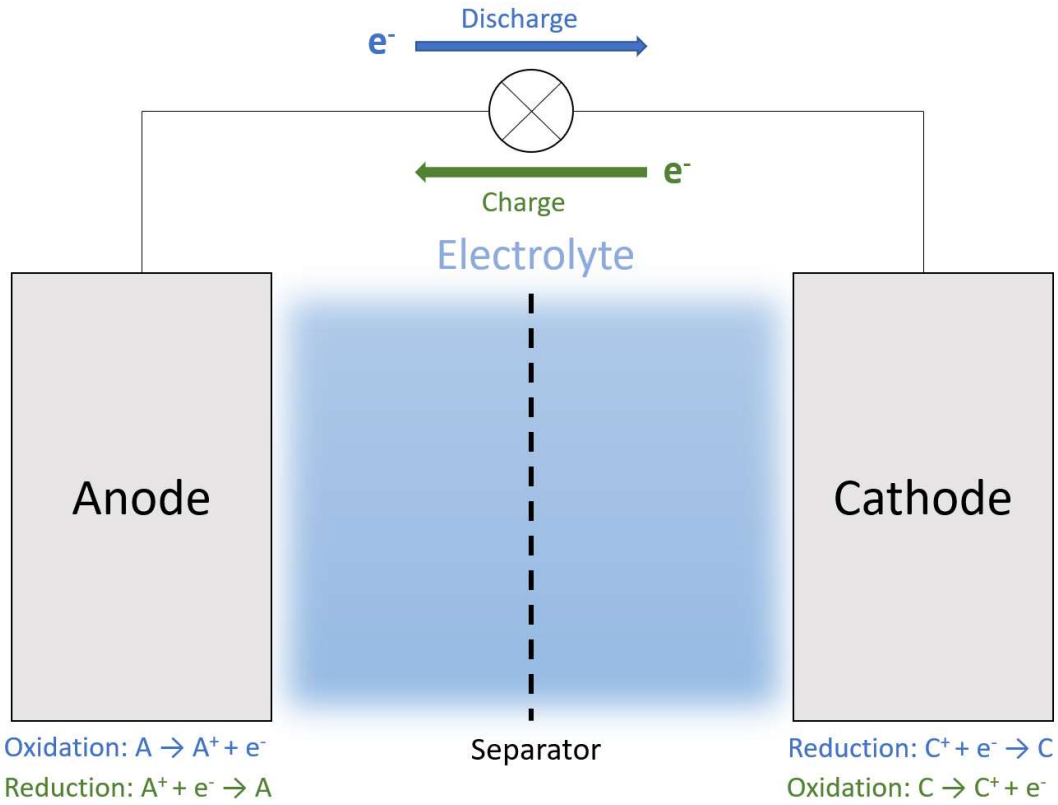

Figure 2.1: Schematic illustration of the components in a battery.

2.1 Lithium ion battery

A lithium ion battery is a good example to show how a battery can function. The anode is typically made from graphite and the cathode is typically a metal oxide made of lithium and transition metals [11]. For example, lithium cobalt oxide ($LiCoO_2$) is a typical cathode material in lithium ion batteries and an illustration of such a battery can be seen in figure 2.2.

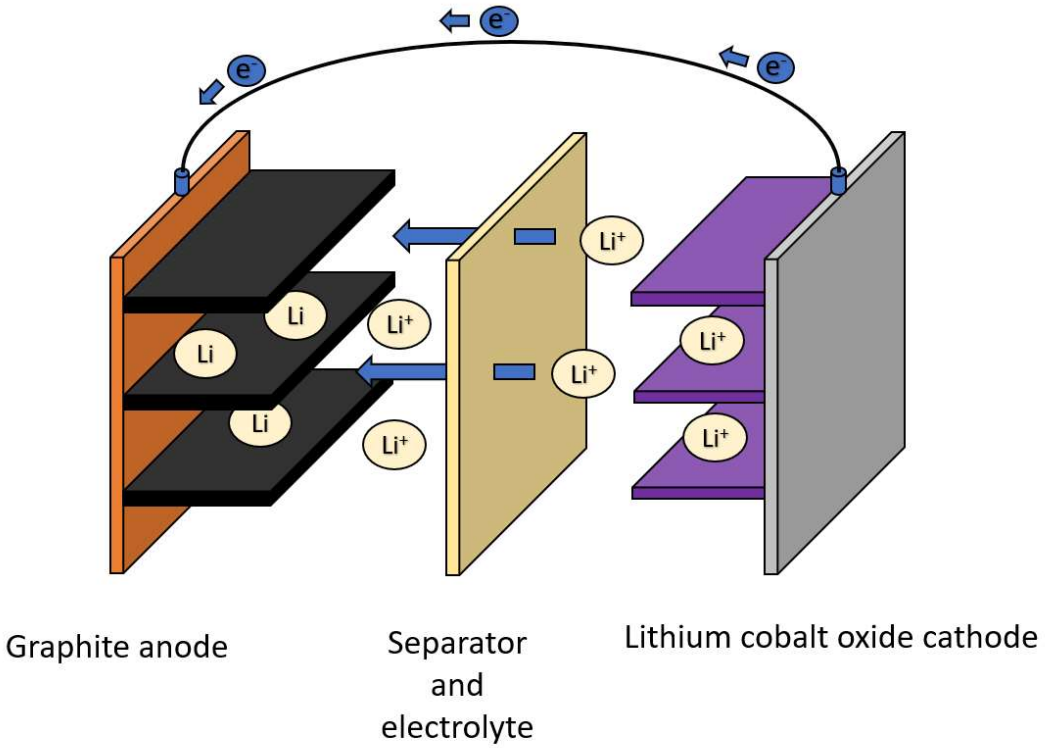

Figure 2.2: Illustration of a lithium ion battery under charging.

When the battery is being charged lithium ions are extracted from the cathode and travel through the separator via the electrolyte, and intercalate into the graphite layers of the anode [11]. This reaction is not spontaneous and thus requires an applied current in the external circuit as a driving force. Through this applied current and the reduction reaction at the anode, both lithium ions and electrons are stored in the anode. While discharging the opposite reaction occurs. Lithium ions leave the anode and intercalates into the cobalt oxide layers. During this reaction there is once again a current in the external circuit. However, in this case the reaction is spontaneous and the current can be used as an energy source. The reactions occurring during charging and discharging at the anode and cathode can be expressed as

$$\text{Cathode side} \qquad \mathrm{LiCoO_2} \underset{\text{discharge}}{\overset{\text{charge}}{\rightleftharpoons}} \mathrm{Li^+ + e^- + CoO_2} \tag{2.4}$$

$$\text{Anode side} \qquad \mathrm{C_6 + Li^+ + e^-} \underset{\text{discharge}}{\overset{\text{charge}}{\rightleftharpoons}} \mathrm{C_6Li} \tag{2.5}$$

As mentioned a lithium ion battery is typically made of materials including lithium, graphite, cobalt, and other transition metals in varying amounts [11]. These materials can often only be extracted in limited regions of the world and come with great economic, environmental, and ethical costs due to the extraction methods and harsh conditions for workers [5, 12]. Graphite

as an anode material also suffers from a relatively low theoretical specific capacity of 372 mAh/g [11], which limits the storage capacity in a battery with a given size or weight requirements. Lithium ion batteries are also known for the safety problem with thermal runaway or even fires due to the volatility and flammability of the organic electrolytes used [4]. However, even with all these problems, lithium ion batteries are still the best performing rechargeable battery technology that we have. In order to keep up with the growing demand for energy storage, as well as to create batteries capable to store greater amounts of energy, we need to look at alternative types of batteries. One alternative type is the zinc-metal battery.

3

Zinc-metal batteries

A zinc-metal battery's working mechanism is similar to the one of a lithium ion battery in the way that it also relies on the transport of ions from one electrode to the other, in order to store energy. However, there are several key differences between the two types of batteries. For one, the ions are now zinc ions and they are divalent, meaning that two electrons will be transferred in the external circuit for each zinc ion. Another key difference is that the anode is a zinc-metal anode. A metal electrode works differently from an intercalation electrode by having the ions deposited on the surface of the electrode instead of intercalation into the electrode. This way of storing the ions leads to a higher theoretical specific energy compared to an intercalation electrode, and the theoretical specific capacity of the zinc-metal is 820 mAh/g [7]. Zinc is also stable in water, allowing the use of aqueous electrolytes which are cheaper and safer compared to the typical electrolytes used in lithium ion batteries.

For the cathode of the zinc-metal battery, there are several different alternatives that have been studied. Some examples are metal oxides, layered sulfides, Prussian blue analogs, and organic materials [13–17]. A zinc-metal battery with a manganese oxide cathode is illustrated in figure 3.1, to exemplify and describe the reactions occurring. A manganese oxide cathode uses intercalation to store zinc ions and it has a theoretical specific capacity of 308 mAh/g [13]. The reaction taking place while charging and discharging can be expressed as

$$\text{Cathode side} \qquad \mathrm{ZnMn_2O_4} \underset{\text{discharge}}{\overset{\text{charge}}{\rightleftharpoons}} \mathrm{Zn^{2+} + 2e^- + 2MnO_2} \tag{3.1}$$

$$\text{Anode side} \qquad \mathrm{Zn^{2+} + 2e^-} \underset{\text{discharge}}{\overset{\text{charge}}{\rightleftharpoons}} \mathrm{Zn} \tag{3.2}$$

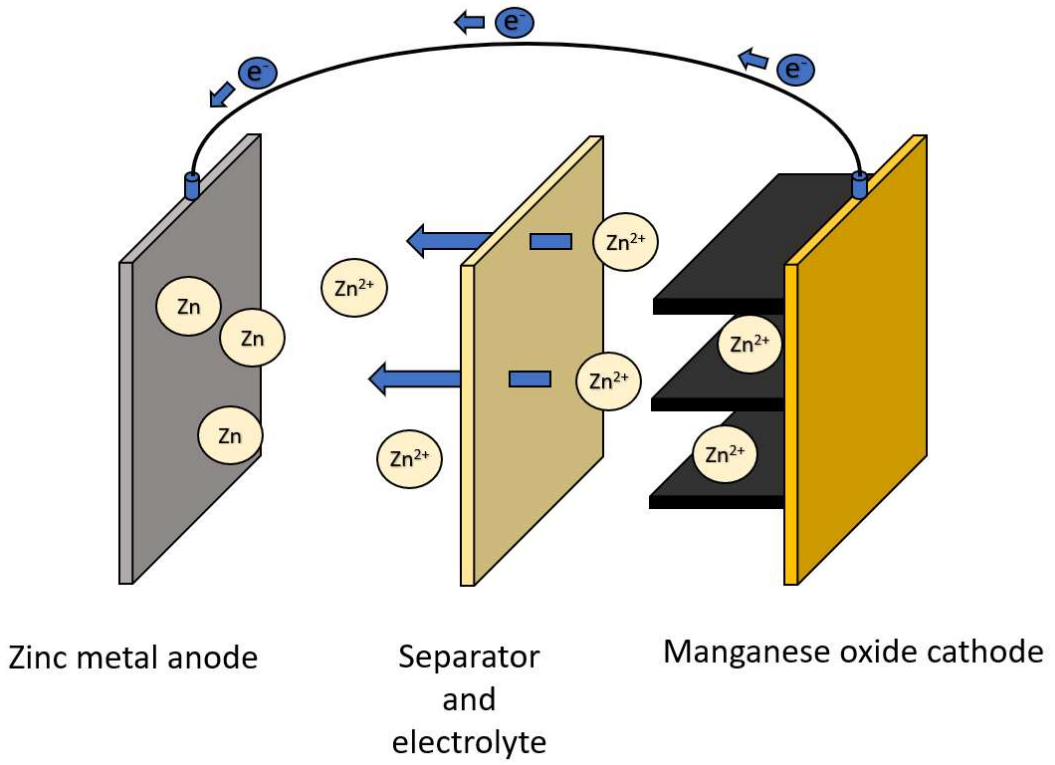

Figure 3.1: Illustration of a zinc-metal battery under charging.

Zinc-metal batteries do have several features that make them a promising candidate for future energy storage applications. The materials used are more abundant, environmentally friendlier, and cheaper compared to lithium ion batteries and also have a higher theoretical energy density [6, 7]. The zinc-metal battery also avoid the thermal runaway problem through the use of aqueous electrolytes. However, zinc-metal batteries are still in the developing phase and there are several problems to sort out before they can be commercialized. One lingering problem that zinc-metal batteries suffer from are a short cycle life. This is due to the growth of dendrites that can potentially short circuit the battery. Initial inhomogeneities on the zinc electrode surface can cause an uneven ion distribution and charge transfer resistance. This will lead to uneven deposition of zinc onto the electrode, and the repeated plating and stripping cycles will amplify the inhomogeneities creating zinc dendrites. These dendrites will eventually penetrate the separator and short circuit the battery [7].

There have been several studies aiming to suppress zinc dendrite growth through the use of different approaches, including promoting epitaxial growth with graphene, coating with a metal oxide to regulate the interfacial interactions or reducing water activity at the electrode surface by adding polymers such as polyethylene oxide [7–9]. However, zinc dendrites continue to be the limiting factor for long life rechargeable zinc-metal batteries.

3.1 Metal deposition

To look at the problems with metal electrodes one can take lithium metal as an example since much effort has been put into the understanding of lithium metal batteries. The main obstacle to overcome for lithium metal electrodes is the growth of lithium dendrites, and the problems caused by them [18]. Figure 3.2 shows an illustration of these problems.

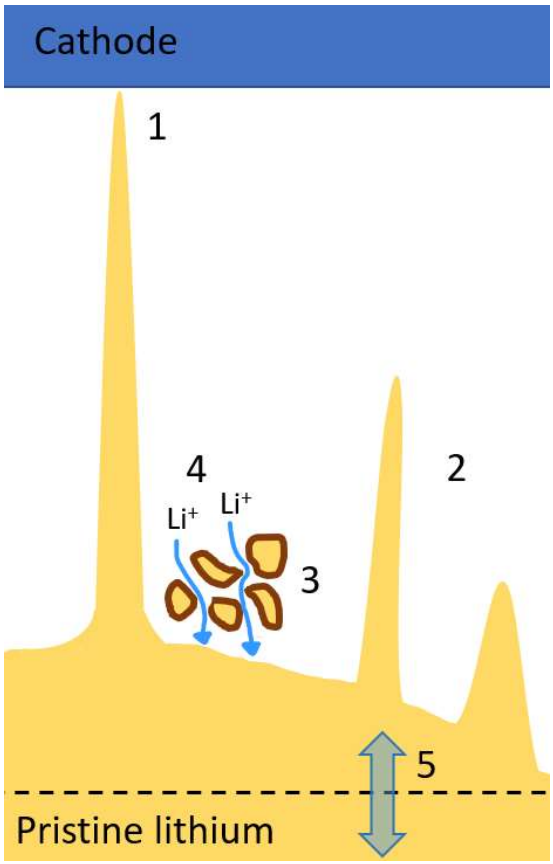

Figure 3.2: Schematic representation of the problems in a lithium metal battery.

(1.) Dendrites can, after repeated cycling, grow large enough to penetrate the separator and reach the cathode. Once the dendrite reaches the cathode it will then act as a pathway for the electrons to travel between the two electrodes, and short circuit the cell [18].

(2.) Due to the growth of dendrites the electrode will experience an increase in surface area. The increased surface area will enhance the side reactions occurring between the lithium metal and the electrolyte. These side reactions consume lithium which in turn lowers the Coulombic efficiency [18].

(3.) The side reactions occurring on the surface of an isolated dendrite creates a solid electrolyte interphase layer that covers the whole dendrite. When this happens the dendrite becomes dead lithium meaning that it is no longer electronically connected to the current collector, and is therefore now electrochemically inert. Since lithium is lost in this process it will also lower the Coulombic efficiency [18].

(4.) The dendrites together with dead lithium create a porous and uneven structure on the surface of the electrode. This structure leads to an increased diffusion pathway and increased resistance for lithium ions and electrons, lowering the energy efficiency of the battery [18].

(5.) During cycling the electrode experiences a large volume change. With repeated cycling this volume change can cause the electrode to lose its mechanical structure which can lead to mechanical failure. The volume change can also change the shape of the electrode in such a way that the electrolyte will no longer fully wet the entire surface.

The zinc-metal electrode suffers from similar problems as the lithium metal electrode does. When the zinc deposits onto the electrode surface it prefers to deposit as platelets with a hexagonal close packed crystal structure [9], as illustrated in figure 3.3. These platelets do not stack in an orderly fashion, instead, they form a porous structure.

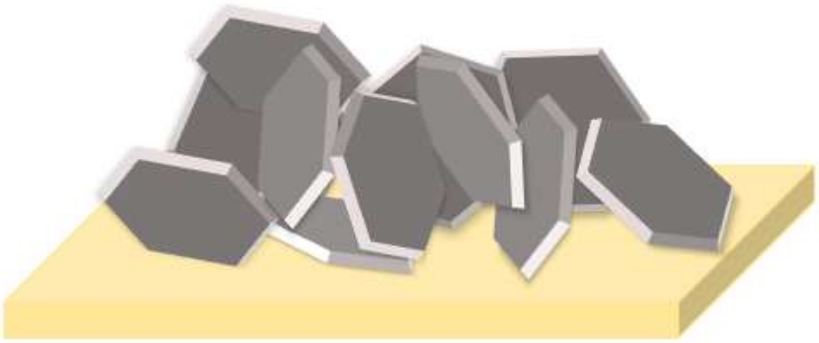

Figure 3.3: Typical deposition behavior of zinc onto an electrode surface.

One method studied to prevent this random stacking of the zinc platelets and to make them stack more uniformly is through the use of graphene. By placing the facets of the graphene perpendicular to the zinc surface a uniform and well structured layer of zinc platelets is achieved. From this first layer, the following layers will be deposited epitaxially and this avoids the porous structure [9]. Another method to achieve uniform zinc deposition is by using a coating layer of metal oxides which will act as solid electrolyte interphase and regulate the interfacial ion behavior. One example of the metal oxide coating is zirconium oxide. By coating the

electrode with zirconium oxide a lower nucleation overpotential is obtained, which leads to more nucleation sites and a more uniform deposition of zinc [8].

3.2 Electrolytes for zinc batteries

The electrolyte plays a vital role on the function and performance of a battery. The main function is enabling the transport of ions between the two electrodes. However, there are several other important requirements for an ideal electrolyte. It should be inert to the electrode surfaces, have high ionic conductivity, have a low electron conductivity, have a wide potential window, and be made out of nontoxic, safe, and cheap materials. For zinc batteries there are several different types of electrolytes and they are generally divided into nonaqueous and aqueous.

One example of nonaqueous electrolytes is a solid polymer electrolyte, which offers a longer cycle life and a high operating temperature range compared to other types of electrolytes. However, solid polymer electrolytes suffer from low ionic conductivity and have poor inteface adhesion with the electrodes. Another example is a gel electrolyte. Gel electrolytes have a higher ionic conductivity compared to the solid polymer electrolyte and they are also more suitable for wearable and flexible electronics due to their flexibility [19].

The aqueous electrolytes are generally divided based on their pH levels. Zinc has an inherent thermodynamic instability in aqueous electrolytes, which results in hydrogen evolution, corrosion, and dendrite growth. This reaction is dependent on the pH level of the electrolyte. In alkaline electrolytes zinc ions can combine with hydroxyl ions near the electrode surface and form zinc oxide. The zinc oxide will then act as a passivation layer and increase the impedance of the battery, slowing down the charge transfer at the interface. The dendrites in an alkaline electrolyte grow in spruce like pattern that can easily pierce through the separator [20].

In neutral and mildly acidic electrolytes the side reactions between the zinc ions and hydroxyl ions are suppressed, due to the lack of hydroxyl ions. However, zinc-metal has a strong tendency to ionize by donating one electron to hydrogen in a water molecule leaving behind a hydroxyl ion. This generation of hydroxyl ions together with the hydrogen evolution, removing the hydrogen from the surface, leads to a build up of hydroxyl ions at the surface which in turn is just like the corrosion of the electrode in the alkaline electrolyte. The dendrites in the neutral and mildly acidic case tend to form hexagonal platelets instead of the spruce like morphology in the alkaline case. This leads to a two dimensional growth on the surface and therefore a longer cycle life. However, the dendrites will still grow and eventually penetrate the separator in this case too [20].

Massive efforts have been put into improving the cycle life of the zinc-metal battery through modification of the electrolyte, mainly trying to suppress the dendrite growth or to change the morphology of the dendrites. One way to achieve this is varying the salt concentration, viscosity, and solvation, in order to modify the transport of ions. There are also studies changing the coordination of the zinc ions in the electrolyte to change the deposition behavior of zinc-metal [20]. Another approach is to reduce the ion transfer kinetics at the surface of the electrode. This was done in one study by adding long chain polyethylene oxide to the electrolyte. The polyethylene oxide attaches to the zinc surface and suppresses the ion transfer kinetics. The suppressed ion transfer kinetics leads to a regulated and uniform distribution of zinc ions at the electrode/electrolyte interface. This results in a uniform deposition of zinc, which increases the cycle life of the battery [7]. In this project, the plan is to use a similar approach by adding sulfated cellulose nanocrystals (CNC) and sodium carboxymethyl cellulose (CMC) to the electrolyte.

4

Methods

To fully understand and evaluate the effect of the additive on the performance of the battery, the first study is how the electrolyte without additives performs. Therefore, the first part of this project is to evaluate electrolytes made out of deionized water and zinc sulfate heptahydrate, with molar ratios shown in table 4.1, using different characterization methods to study their properties. The physical properties such as the ionic conductivity, density, viscosity, infrared, and Raman spectra were measured. Once the physical properties were known, symmetric zinc cells and zinc/copper cells were assembled to investigate the cycling stability and the Coulombic efficiency. After the full characterization of the aqueous electrolytes was performed, the optimal concentration was chosen to serve as the base composition for investigating the role of the additives. The additives CNC and CMC were added at a weight percentage of 0.1wt%, and the same characterization was then conducted for these new electrolytes. The final step was to disassemble the cells that have been cycled and to study the morphology of zinc deposit by scanning electron microscopy (SEM).

Table 4.1: Molar ratios of water and zinc sulfate in the electrolytes used in this project.

Electrolyte	Molar ratio of H_2O to $ZnSO_4$
#1	15
#2	25
#3	50
#4	200
#5	500

Table 4.2: Amount of added additives to electrolyte #2.

Additive	Added amount [wt%]
CNC	0.1
CMC	0.1

4.1 Ionic conductivity

The ionic conductivity is an important property of the electrolyte as this determines how well the electrolyte can transport ions between the electrodes. In this project the ionic conductivity was measured with a broadband dielectric spectrometer from Novocontrol. The broadband dielectric spectrometer works by applying an external alternating electric field and sweeping the frequency over a certain range (in this project $10 - 10^7$Hz). During the frequency sweep, it measures the response from the sample which is used to calculate the conductivity. Measurements were performed between the temperatures 0°C-40°C with 5°C intervals in order to see how the conductivity depends on temperature.

4.2 Density and viscosity

The density and viscosity of the electrolytes were measured with an Anton Paar DMA 4500 M with a lovis 2000 M/ME microviscometer module. The density was measured by filling an u-shaped glass tube with the electrolyte and finding the characteristic frequency, which relates to the density of the sample. After reaching a stable oscillation it is switched off and the oscillation fades out. By repeating this procedure a highly accurate value for the density is obtained [21]. The viscosity was measured by filling a straight glass tube with the electrolyte and letting a small steel ball sink through the tube. By knowing the inner diameter of the tube, the diameter of the ball, and the time it takes to sink through a fixed distance, the viscosity can be obtained.

4.3 Infrared spectroscopy

In infrared spectroscopy, a sample is exposed to photons with energies in the infrared range. These photons may excite vibrational states of the bonds in the sample. Since the vibrational state is unique for each bond, infrared spectroscopy can be used to identify the type of bonds present in the sample. For a vibration to be detected in infrared spectroscopy it must change the molecular dipole moment [22]. In this project infrared spectra were measured with a Bruker Optics IFS 66v/S Vacuum FT-IR in the range 500-4000 cm^{-1} with a step size of 2 cm^{-1}.

4.4 Raman spectroscopy

In Raman spectroscopy monochromatic light interact with the material and the molecules are excited to a virtual state between the highest vibrational state and the next electronic state. When the molecule relaxes it can fall back to the same energy state (Rayleigh scattering), a higher energy state (Stokes scattering), or a lower energy state (anti-Stokes scattering). This

can be seen in figure 4.1. For a vibration to be detectable in Raman spectroscopy it must change the polarizability of the molecule. Therefore, Raman and infrared spectroscopy are often seen as complementary methods [22]. In this project the Raman spectrum was measured with a Dilor XY 800 with a 514 nm laser.

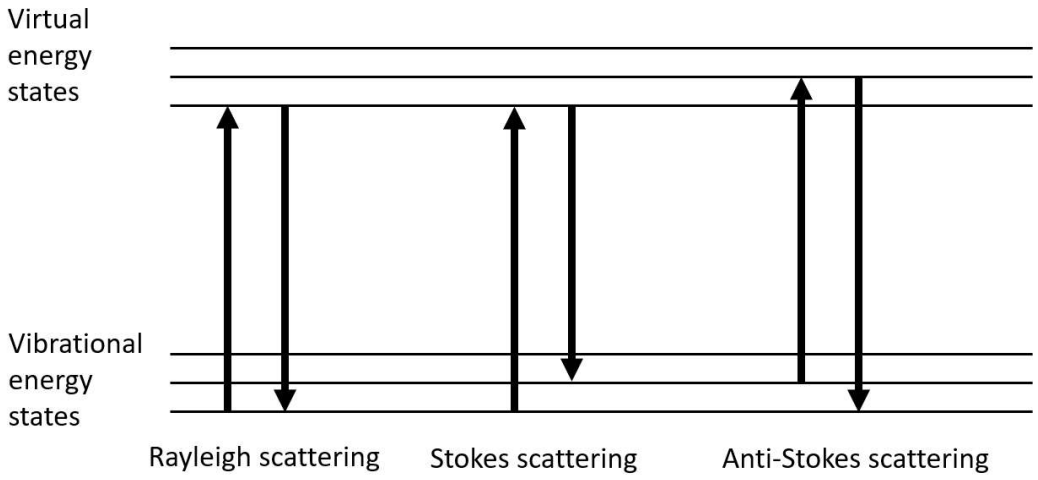

Figure 4.1: Illustration of the different scattering processes occurring in Raman spectroscopy.

4.5 Electrochemical measurements

Coin cells were assembled to test the electrochemical performance of the electrolytes. Two different types of coin cells were built during this project, symmetric zinc/zinc cells, and zinc/-copper cells. An illustration of the components in a coin cell can be seen in figure 4.2. The separator used was three layers of filter paper from VWR with a thickness of around 130 µm. The zinc foil used was from Goodfellow and the copper was from Schlenk. All measurements on these coin cells were performed on a Scribner 580 battery test system.

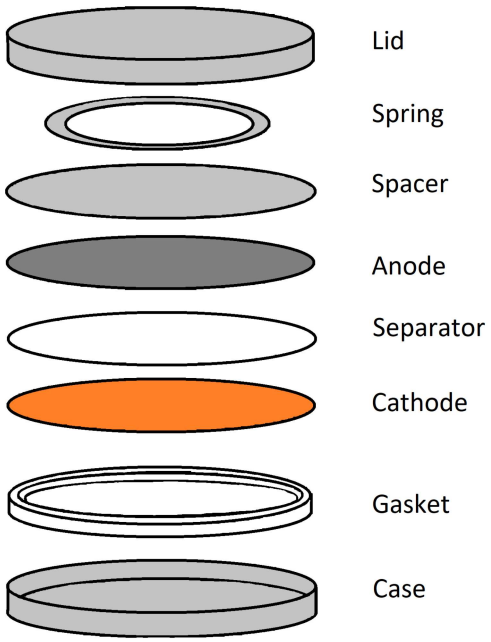

Figure 4.2: Schematic of the components of a coin cell.

4.5.1 Symmetric zinc/zinc cell

In a symmetric zinc/zinc cell both of the electrodes are made out of zinc. These cells were used to study the cycling stability and how the different electrolytes affect the stability. In this project, the cycling stability was studied by two different electrochemical methods, one with an increasing current density and one with a constant current density. In the protocol with the increasing current density the capacity plated and stripped is kept constant while the current density increases. At the start a current density of 2 mA/cm^2 was applied for 1 hour of plating and stripping for 10 cycles. After that, a current density of 5 mA/cm^2 was applied for 24 minutes of plating and stripping for another 10 cycles. Lastly, 10 mA/cm^2 was applied for 12 minutes of plating and stripping until the cell short circuited. The second protocol used was plating and stripping at a constant current density, both 1 mA/cm^2 and 5mA/cm^2 were used. For 1 mA/cm^2, there was plating and stripping for 60 minutes each. For 5 mA/cm^2, there was plating and stripping for 30 minutes each. Both cells were cycled until short circuit.

4.5.2 Zinc/copper cell

In a zinc/copper cell, the counter electrode is zinc and the working electrode is copper. This cell was used to evaluate the Coulombic efficiency of plating and stripping of zinc. The protocol used follows the one described by Brain D. Adams et al as method 3 [23], and is illustrated in figure 4.3. The initial conditioning of the copper electrode was conducted by plating at 0.5 mA/cm^2 for 4 hours and then stripping this until a cutoff voltage of 0.4 V is reached. After

that the same amount of zinc was plated on the copper electrode. With this plated zinc layer on the copper electrode was cycled with lower areal capacity. These cycles stripped and plated zinc at 0.5 mA/cm^2 for 30 minutes each for 10 cycles. After the cycling a final stripping was performed until a cutoff voltage of 0.4 V. The Coulombic efficiency was then calculated with the following equation

$$CE = \frac{10Q_c + Q_f}{10Q_c + Q_i} \tag{4.1}$$

where Q_c is the plated and stripped capacity during the repeated cycles, Q_f is the capacity stripped at the end and Q_i is the initial plated capacity.

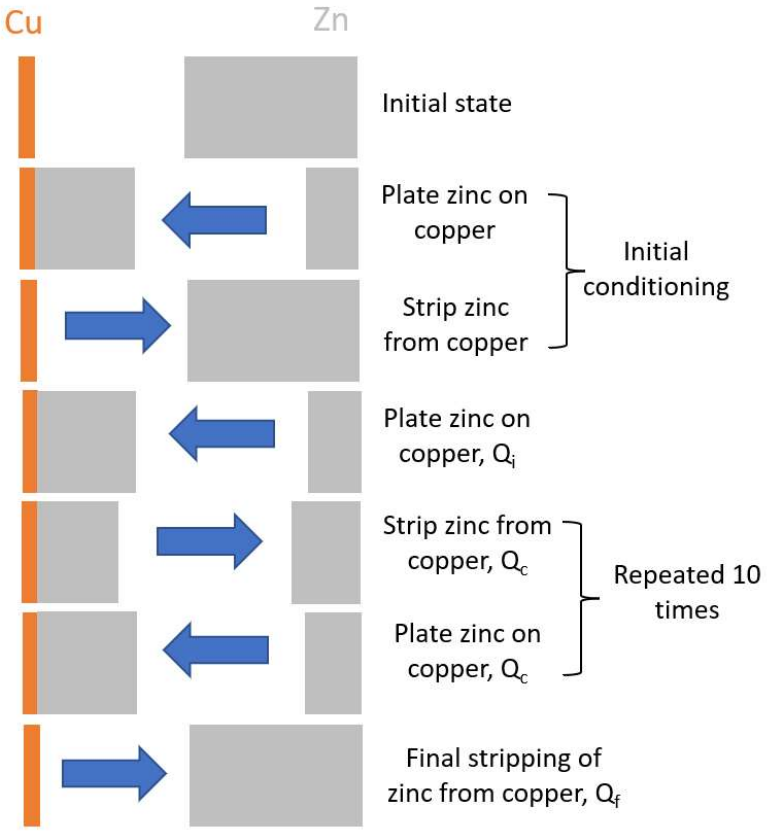

Figure 4.3: Illustration of the zinc plating and stripping protocol in the zinc/copper cell to determine the Coulombic efficiency.

4.6 Scanning electron microscopy

In SEM, a focused electron beam is scanned across the surface of a sample. A part of the electron beam will be reflected as secondary electrons, these are collected and the intensity is recorded. By measuring the intensity for each position of the scan and then combining all the measurements one can create a high resolution image of the sample surface. In this project,

SEM was used to study the morphology of the zinc deposition on both a zinc surface as well as a copper surface. The cycling that was performed before the SEM measurements for the symmetric cell was to plate and strip at 2 mA/cm^2 for 1 hour each and repeat this for 10 cycles. For the zinc/copper cell, plating at 0.5 mA/cm^2 for 4 hours and then stripping until a cutoff voltage of 0.4 V was performed, and then plating again at 0.5 mA/cm^2 for 4 hours. The cells were then opened and the electrodes were washed and dried before being transferred into the SEM. A JOEL JSM-7800F Prime FEG was used to collect images of the electrode surfaces. The voltage of the electron beam was 5 keV and the exposure time was 77 seconds.

5

Results and discussion

5.1 Physical characterization of electrolytes

5.1.1 Ionic conductivity, viscosity, and density

The results from the conductivity measurements are shown in figure 5.1. The conductivity goes up with increasing salt concentration, that is, lowering the molar ratio of H_2O to $ZnSO_4$ from 500:1 of electrolyte #5 to 25:1 of electrolyte #2 up until 15:1 of electrolyte #1 where it goes down. From table 5.1 it shows that there is a big increase in viscosity when comparing electrolyte #1 to electrolyte #2, and this can be the reason for the decrease in conductivity. Another aspect to keep in mind for all measurements on electrolyte #1 is that the concentration is over the saturation limit of zinc sulfate in water at room temperature. This leads to the formation of crystals in the solution, which might make the measurements inaccurate. The behavior of the forming crystals can be seen in figure 5.2 together with the other electrolytes as well. From table 5.2 one can also see that the density of the electrolytes increases with increasing concentration of zinc salt.

Based on these results electrolyte #2 was chosen to serve as a base for the addition of the additives. It has the highest conductivity and a high salt concentration while avoiding the problem of the saturation limit as seen in electrolyte #1. Having a high salt concentration has been shown to improve the stability of the cells by lowering the concentration gradient near the surface [24]. This behavior of improved stability is further demonstrated in section 5.2.

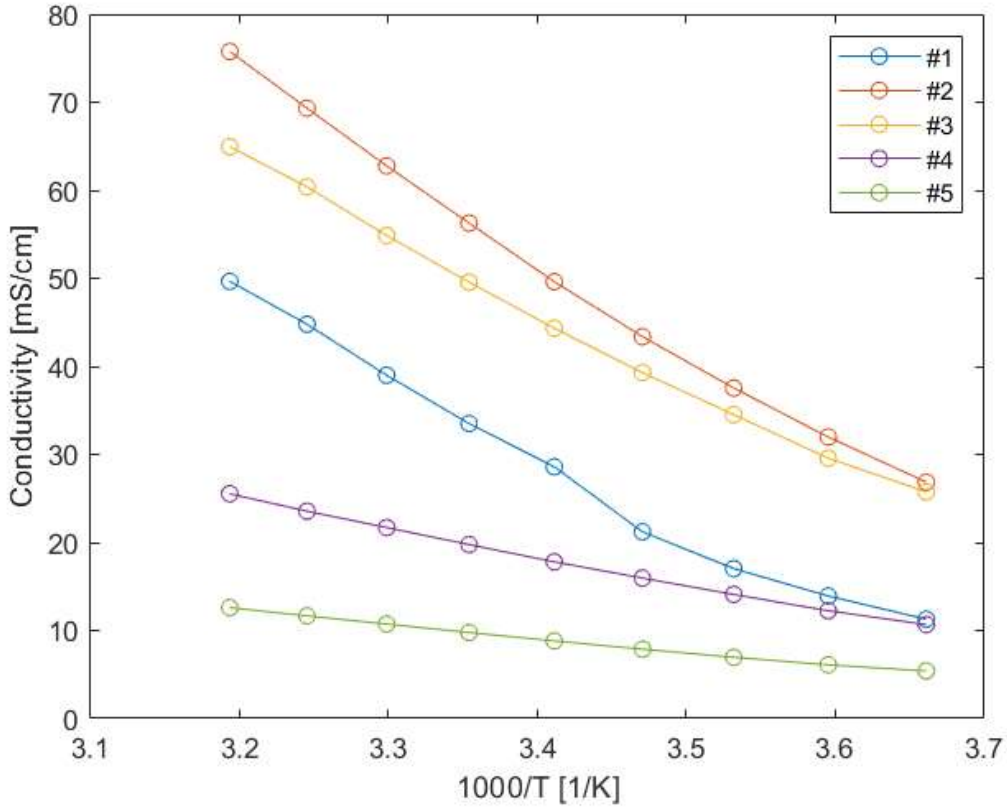

Figure 5.1: Conductivity of the electrolytes between 0°C-40°C.

Table 5.1: Viscosity of electrolytes at 20°C.

Electrolyte	Viscosity at 20°C [mPas]
#1	13.0
#2	4.6
#3	2.1
#4	1.2
#5	1.1

Table 5.2: Density of electrolytes at 20°C.

Electrolyte	Density at 20°C [g/cm^3]
#1	1.51
#2	1.34
#3	1.17
#4	1.05
#5	1.02

Figure 5.2: Photo of electrolytes lined up with #1 to the far left and #5 to the far right.

These measurements were then repeated for electrolytes with the additives. From the conductivity measurement in figure 5.3, the conductivity of the electrolytes were only slightly affected by the additives, with a small increase with the addition of CNC and a small decrease with CMC compared to electrolyte #2. An increase in viscosity was obtained with the addition of CMC, as can be seen in table 5.3. It is worth noting that the viscosity of the electrolyte containing CNC has not been included since the CNC particles aggregated during the measurement. This led to every measurement having a higher value than the previous one until it reached the point where the steel ball no longer could travel through the tube and got stuck. Thus, no reliable value of the viscosity was obtained for this electrolyte. Table 5.4 shows the results of the density measurement and with the additives, and from it a very slight decrease in density is observed compared to the base electrolyte #2.

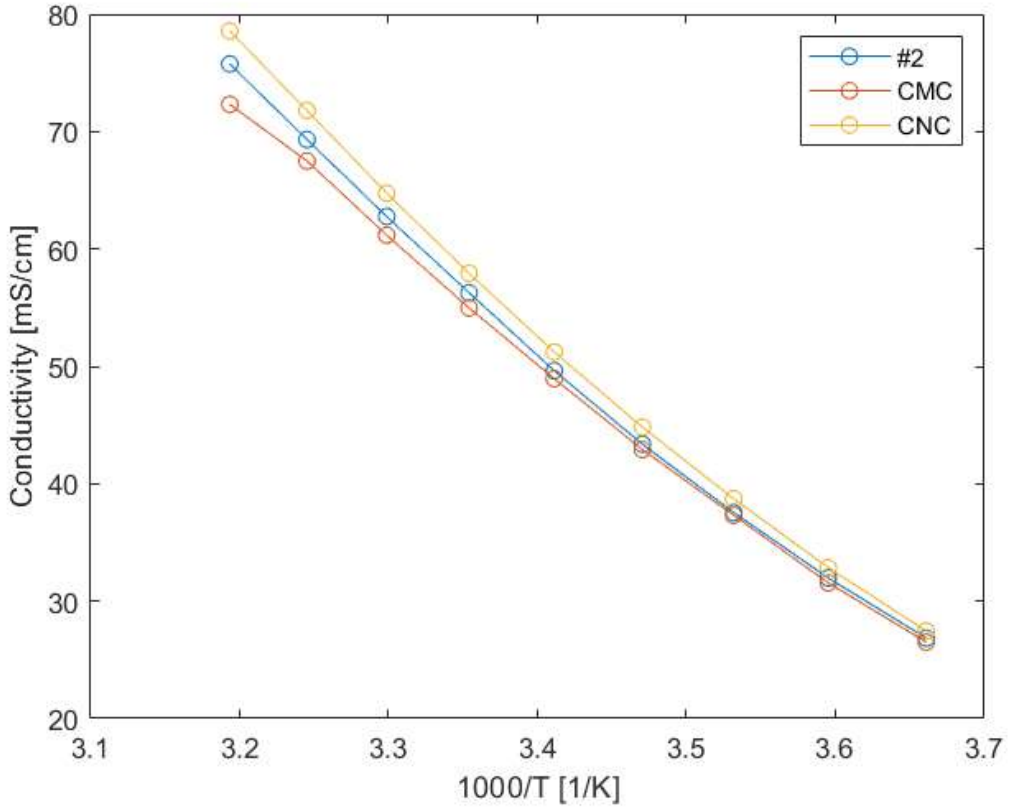

Figure 5.3: Conductivity of electrolyte #2 and the electrolytes containing CMC and CNC between 0°C-40°C.

Table 5.3: Viscosity of electrolyte #2 and electrolytes containing CMC at 20°C.

Electrolyte	Viscosity at 20°C [mPas]
#2	4.6
CMC	6.1

Table 5.4: Density of electrolyte #2 and electrolytes containing CMC and CNC at 20°C.

Electrolyte	Density at 20°C [g/cm^3]
#2	1.34
CMC	1.33
CNC	1.33

5.1.2 Infrared and Raman spectroscopy

As shown in figure 5.4, three main peaks are found in the infrared spectrum. The peak between 2700 cm^{-1} and 3700 cm^{-1} is the O-H stretching and the peak at 1600 cm^{-1} is the H-O-H

bending of the water molecule. The peak at 1100 cm^{-1} is the antisymmetric stretching of the sulfate ion and a clear increase of the absorbance is shown with increasing salt concentration. In figure 5.5 the Raman spectra are shown, and as in the infrared spectra the O-H stretching and H-O-H bending as well as the antisymmetric stretching of the sulfate ion can be seen. However, there are also peaks corresponding to the bending and stretching of the sulfate ion. A strong fluorescence background for the electrolytes is seen in the Raman spectra. The origin of this background is not entirely clear and could be related to contaminants in the solution or undissolved salt crystals.

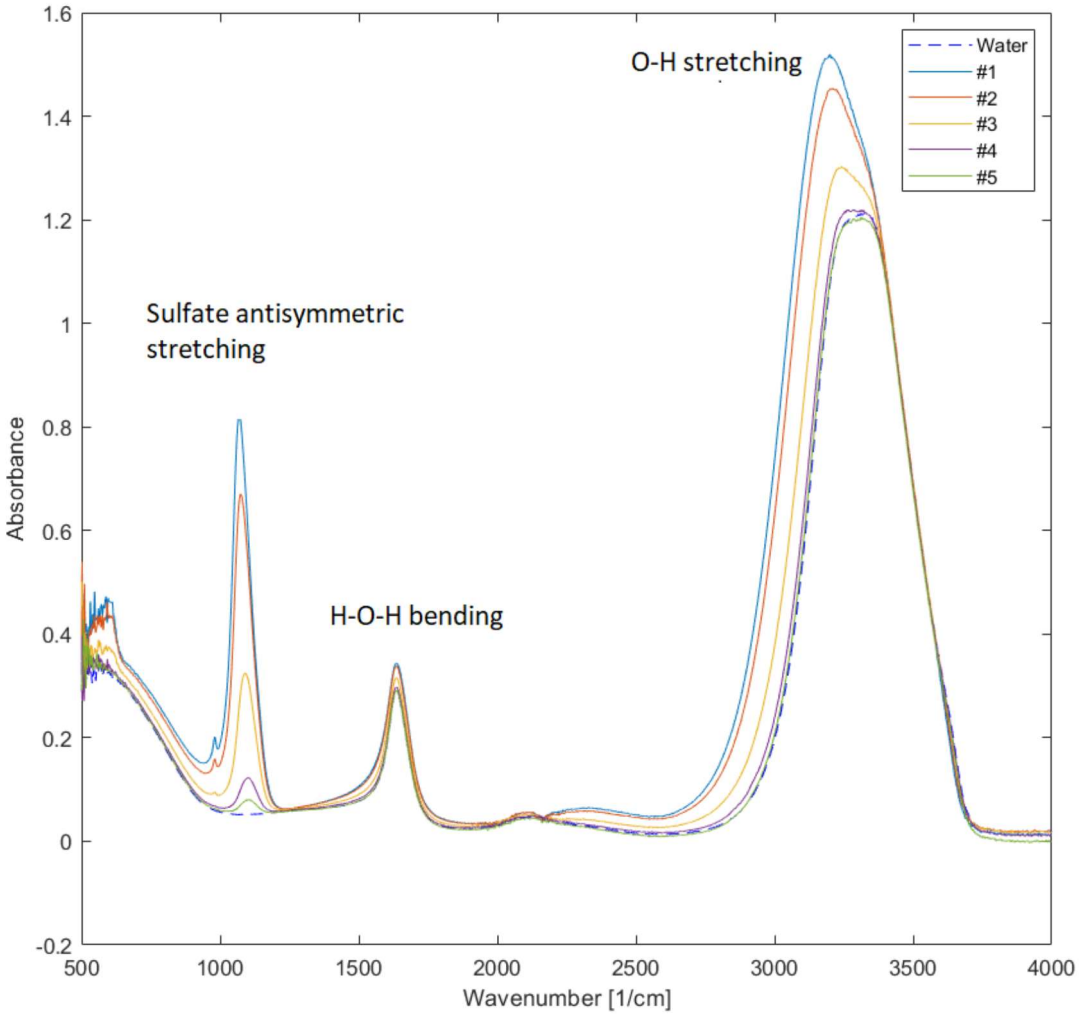

Figure 5.4: Infrared spectra of electrolytes #1-#5 and deionized water.

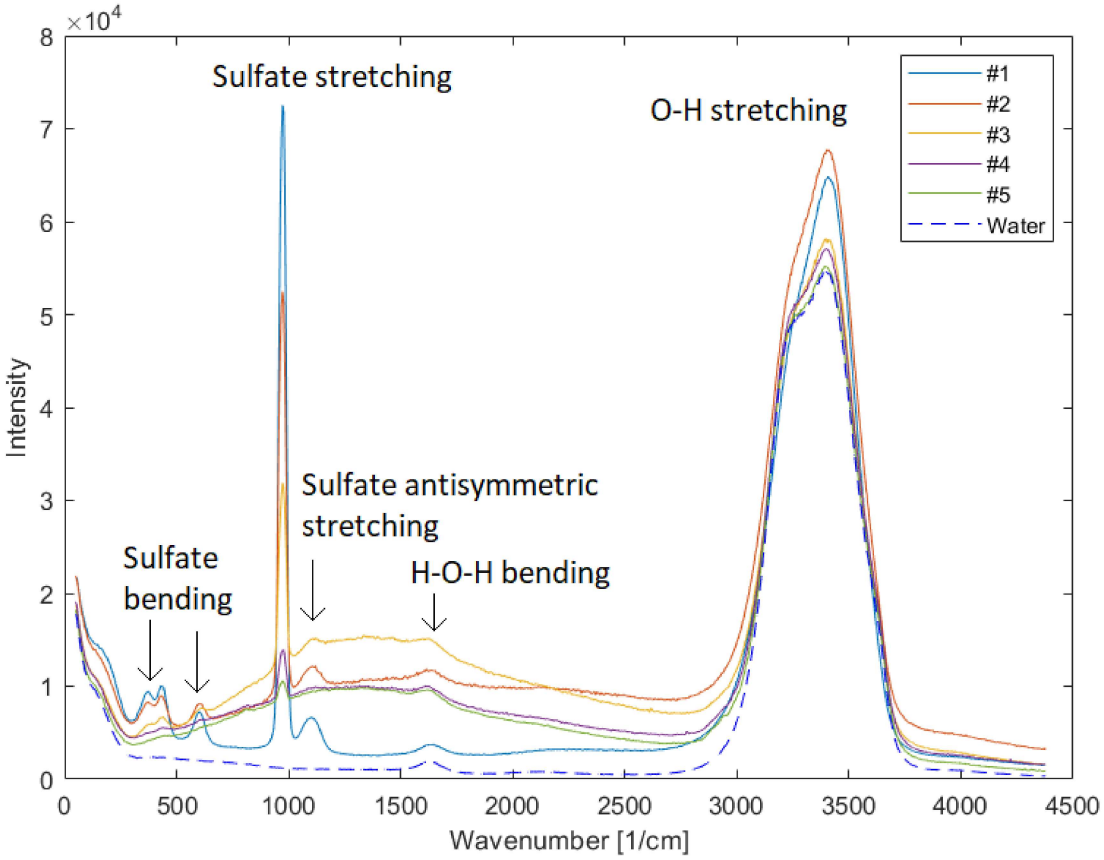

Figure 5.5: Raman spectra of electrolytes #1-#5 and deionized water.

Figure 5.6 shows the infrared spectra for the electrolytes with the additives and the #2 electrolyte. There are no new peaks or any shift in the wavenumber of the preexisting peaks. The only thing to note is the decrease in absorbance.

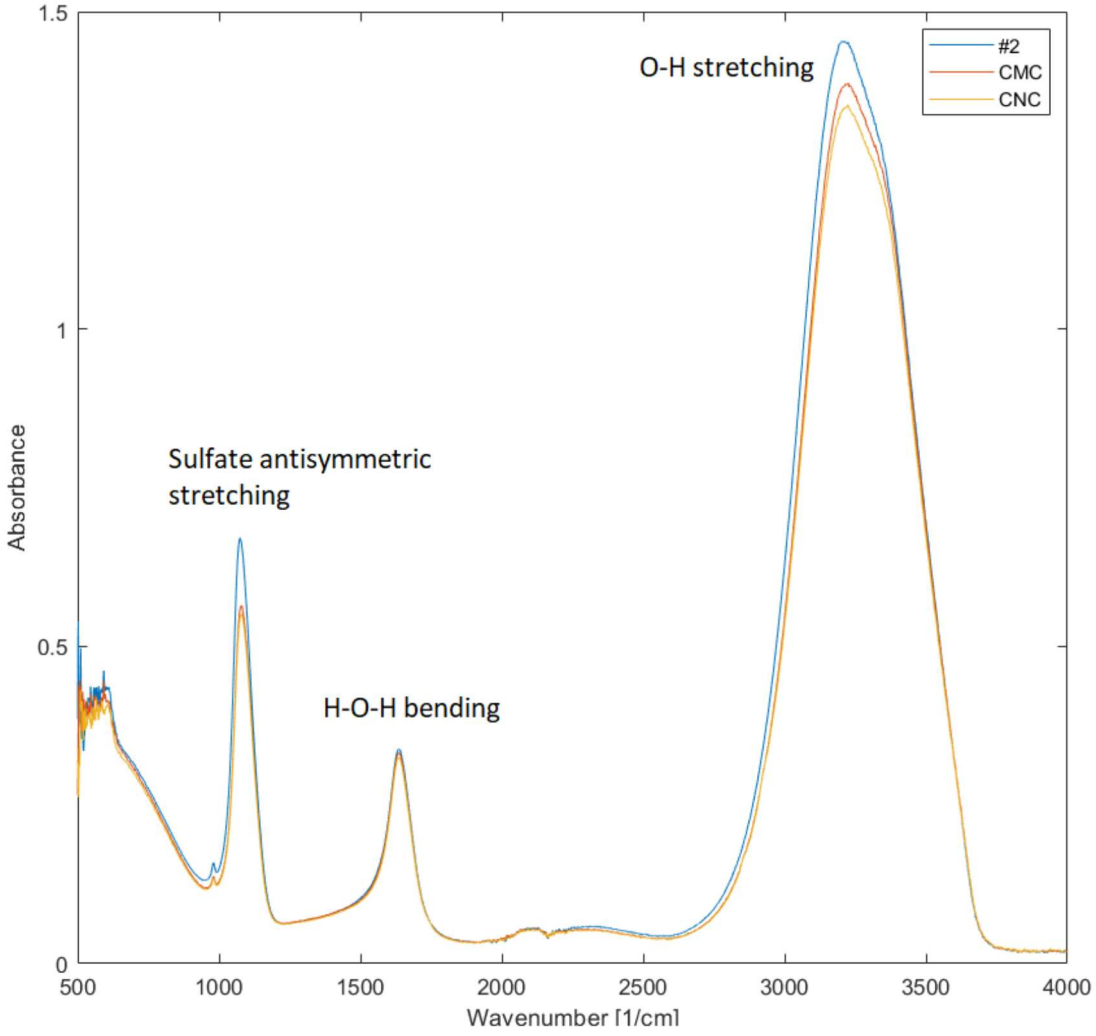

Figure 5.6: Infrared spectra of electrolyte #2 and electrolytes containing CMC and CNC.

5.2 Electrochemical measurements

5.2.1 Symmetric zinc/zinc cell

The effect of the concentration on the cycling stability of symmetric cells is shown in figures 5.7 and 5.8. For the measurement in figure 5.7 and 5.8 the cycling protocol with plating and stripping at a constant current density was used with current densities 1 mA/cm^2 and 5 mA/cm^2 respectively. Figure 5.7 shows that electrolyte #2 and electrolyte #3 were able to sustain the cycling for considerably longer than the cells with other electrolytes, both lasting over 700 hours. Electrolyte #4 and #5 have lower salt concentration and thus they experience greater concentration gradients near the surface [24]. This will induce preferred deposition of zinc on the top of dendrite structures, promoting the growth of dendrites. Therefore, a faster

penetration of the separator can be expected, which leads to earlier short circuit. The poor performance of electrolyte #1, might be attributed to crystals forming in the electrolyte since the salt concentration is over the saturation limit. These crystals could cause problems for the cycling in several ways. They might block and decrease the usable electrode surface, they might hinder the transport of ions in the electrolyte, or they might increase the dendrite growth. It is also seen from electrolyte #3 that the overpotential was increasing before the short circuit of the cell. This behavior is not seen for electrolyte #2 and this could indicate that the zinc deposition with electrolyte #3 created a higher interface resistance during long term cycling compared with electrolyte #2.

Figure 5.8 further demonstrates the stable cycling with electrolyte #2 and #3. For the cell with electrolyte #1 cycling under high current density, it does not fail due to a short circuit but instead, it is not possible to plate and strip the full capacity. This is evident from the voltage spikes at the end of the plateaus which suggest that the plating or stripping reaction was not sustained for the whole cycle. For the cells with electrolyte #4 and #5 it is seen that the cells fail to sustain the cycling already from the first cycle, this is likely due to the electrode/electrolyte interface being unstable. A closer look at the start of the cycling it shown in figure 5.9.

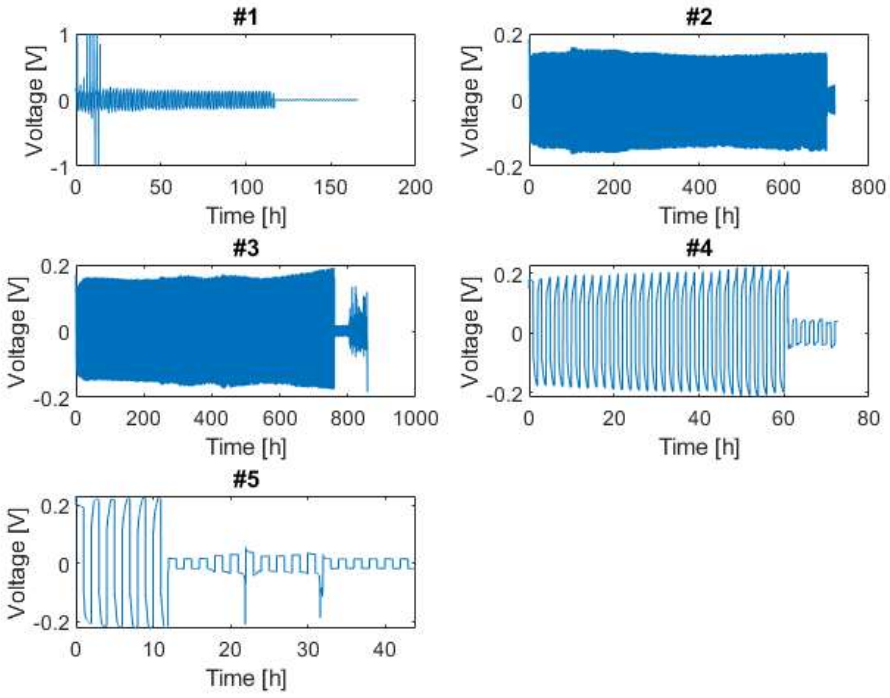

Figure 5.7: Cycling profiles for symmetric cells with electrolytes #1-#5, with plating and stripping at 1 mA/cm^2 for 1 hour each until short circuit.

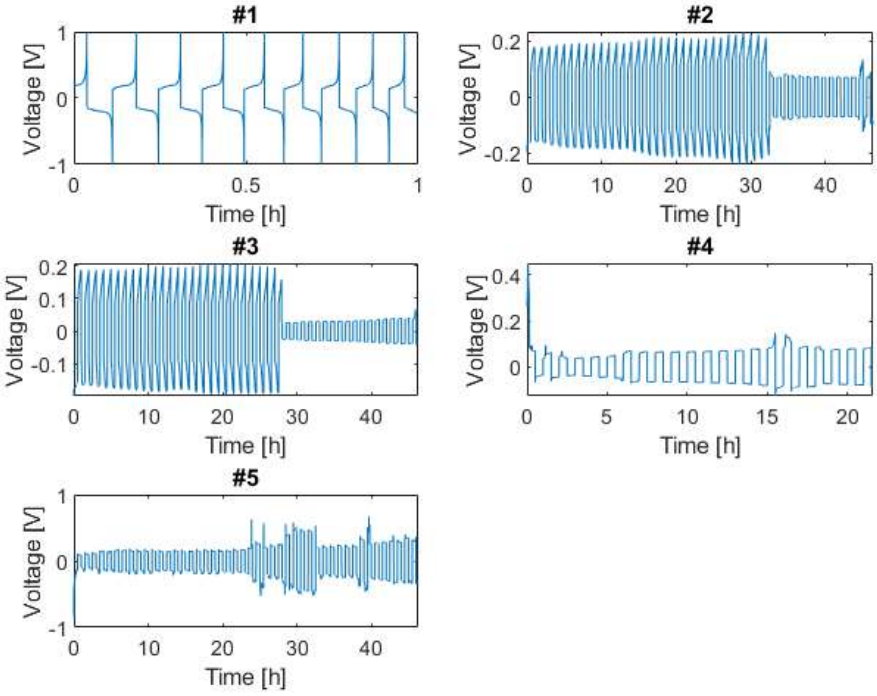

Figure 5.8: Cycling profiles for symmetric cells with electrolytes #1-#5, with plating and stripping at 5 mA/cm^2 for 30 minutes until short circuit.

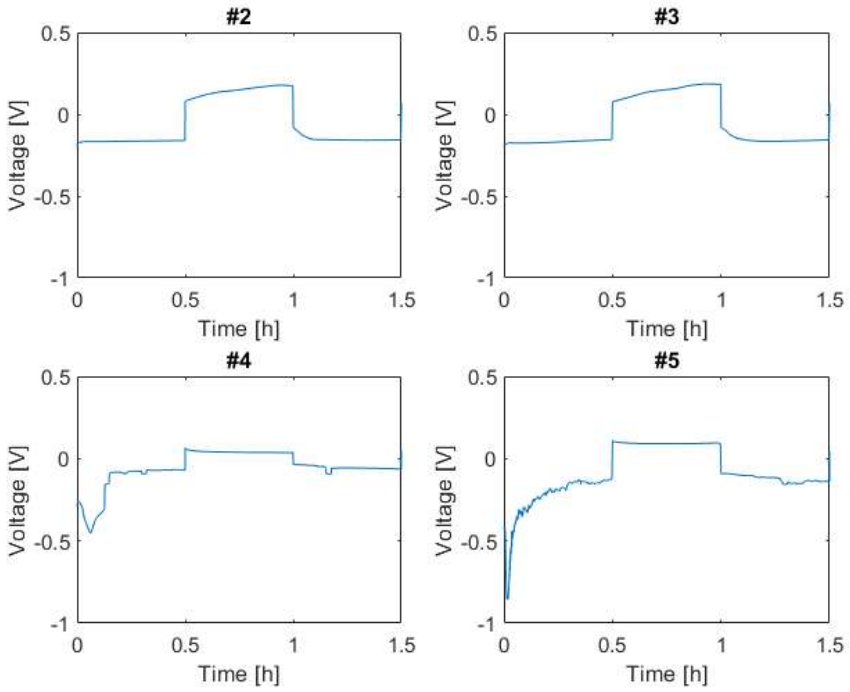

Figure 5.9: Close up of the initial cycling in figure 5.8.

Figure 5.10 shows the effect of the additives on the stability of the symmetric cells. The cycling protocol used was the one with a constant current density of 5 mA/cm^2. The addition of CNC shows no improvement to the cycling stability and the time for short circuit of the cell is roughly the same as that with electrolyte #2. However, the addition of CMC remarkably improves the cycling stability of the cell.

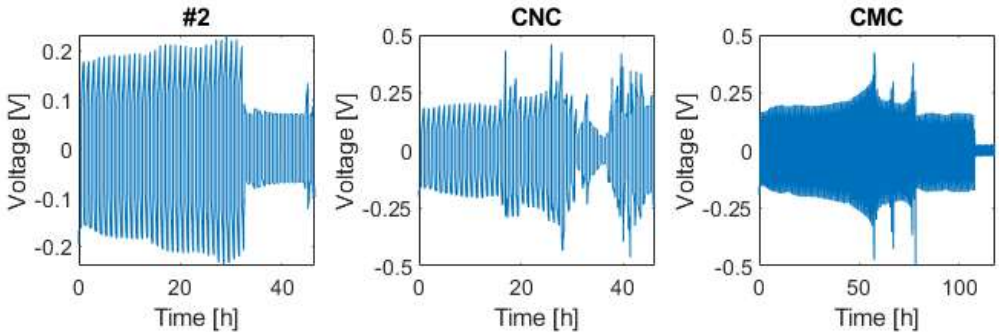

Figure 5.10: Cycling profiles for symmetric cells with electrolyte #2 and with electrolytes containing CMC and CNC, with plating and stripping at 5 mA/cm^2 for 30 minutes until short circuit.

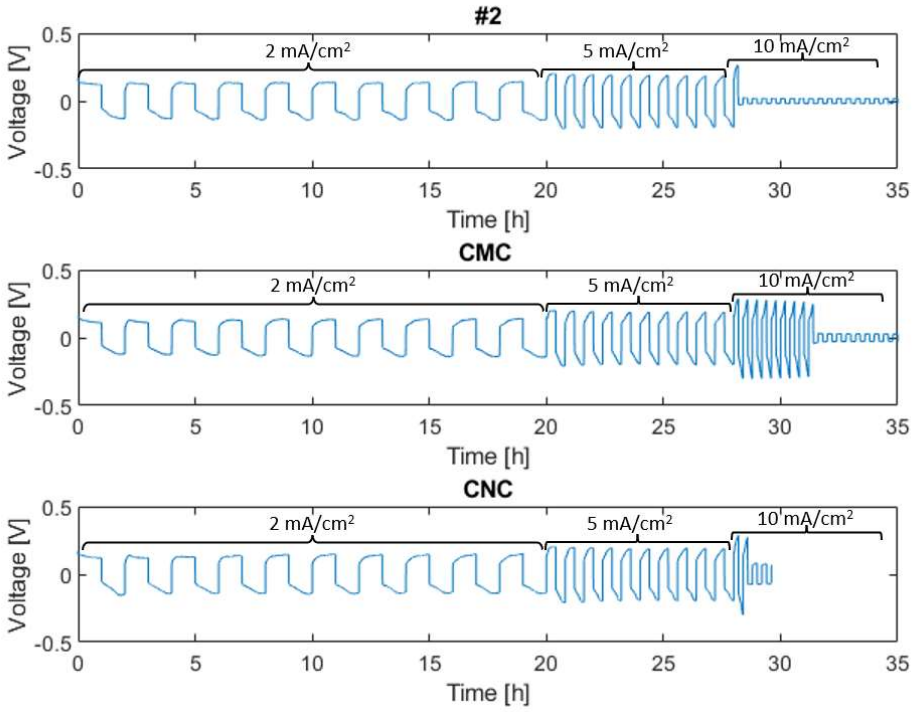

Figure 5.11: Cycling profiles for symmetric cells with electrolyte #2 and with electrolytes containing CMC and CNC, with constant plating and stripping capacity and increasing current density.

The impact of CMC addition is confirmed in figure 5.11, cycling at increasing current density. The cells with electrolyte #2 and the electrolyte containing CNC both short circuit at 10 mA/cm^2, while the electrolyte containing CMC could cycle at this high current density.

5.2.2 Zinc/copper cell

The Coulombic efficiency was measured in the zinc/copper cells with the protocol proposed by Brain D. Adams et al [23] and details are described in section 4.5.2. The motivation for using this protocol instead of other standard methods, like repeated plating and stripping, is to reduce the capacity loss due to reactions with the copper surface. By using this method it focuses on the capacity loss induced by the electrolyte, which is the main goal of this project. One thing to note though is that the Coulombic efficiency is partly dependent on the plating and stripping capacity and the number of cycles. To compare values for different electrolytes the measurement should be carried out with the same protocol. Figure 5.12 shows the results of the Coulombic efficiency measurement for electrolytes #1-#5. The cell with electrolyte #3 delivers the highest Coulombic efficiency, 96.6%, with the electrolyte #2 just slightly lower with a Coulombic efficiency of 96.5%. It is worth noting that the result for electrolyte #1 is not accurate as it can be seen from the cycling profile, that the protocol is unable to be performed as intended.

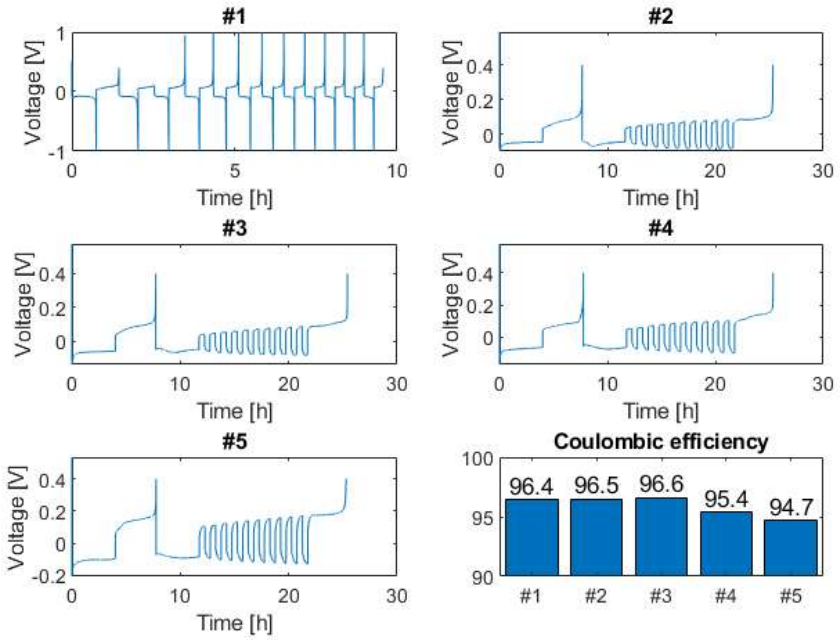

Figure 5.12: Cycling profiles and Coulombic efficiency for the zinc/copper cells with electrolytes #1-#5.

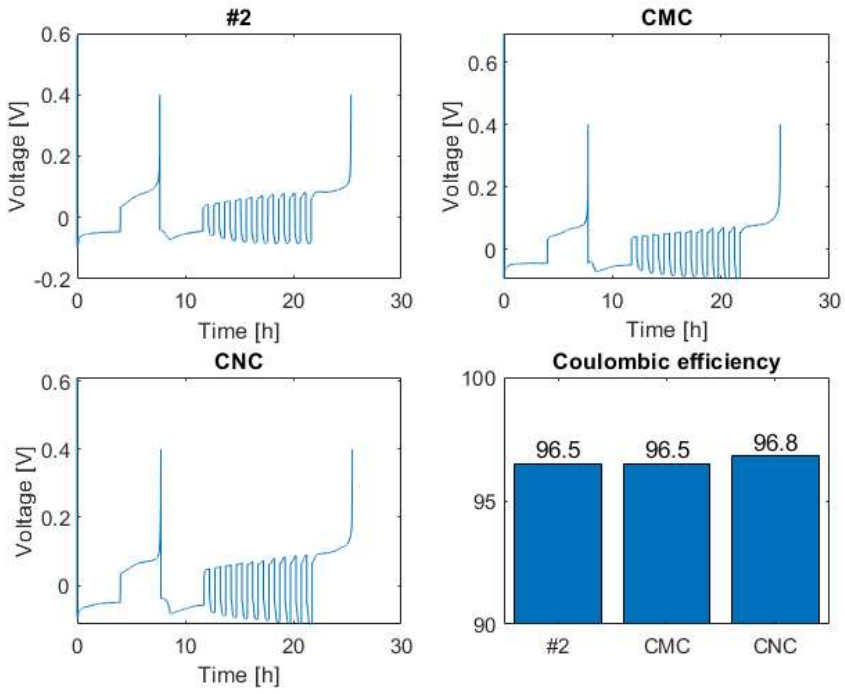

Figure 5.13: Cycling profiles and Coulombic efficiency for the zinc/copper cells with electrolyte #2 and electrolytes containing CMC and CNC.

The effect of the additives CNC and CMC on the Coulombic efficiency can be seen in figure 5.13. Cells with electrolyte #2 and with addition of CMC performed at a similar level whereas the addition of CNC improved the performance, which in contrast to the results of previous stability tests.

5.3 SEM imaging

Images of pristine copper and zinc surfaces are shown in figure 5.14 and they can be used as a reference for analyzing the images of surfaces with deposited zinc.

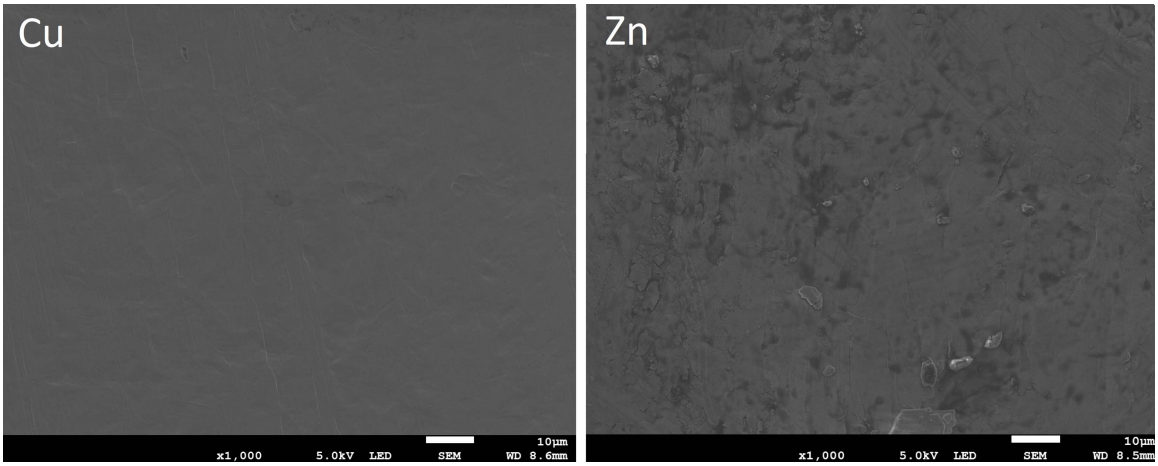

Figure 5.14: Images of copper and zinc electrodes before plating/stripping.

The images of zinc deposition onto a zinc electrode with the electrolytes #2, #4, and #5 are shown in figure 5.15. It is important to note that the cell with electrolyte #4 short circuited after 3 cycles and the one with electrolyte #5 was unable to plate even at the first cycle, which can be seen in figure 5.16. The images of zinc cycled with the electrolyte #2 show that zinc prefers to deposit in hexagonal platelets as previously reported [20]. The size of these platelets are ranging from less than 1 µm to more than 10 µm and they stack without any order. In the images of the sample with electrolyte #4, most of the surface is not covered by zinc platelets and looks similar to the pristine zinc surface. This is most likely due to the cell short circuiting after only a few cycles and thus it leaves less time for zinc to deposit. However, since the cell short circuited from a dendrite piercing through the separator one could expect to see large dendrite like structures, but there are few large structures to be seen. One explanation for this could be that during the removal of the separator all large dendrites also got removed. However, it is worth noting that a structure of roughly 10 µm is shown in the middle image and that the short circuit could possibly be caused by structures of this size. For the electrolyte #5, the cell was unable to complete a full cycle and there are no platelets on the surface. However, it does look like the electrode itself has become porous and platelets have grown inside of the electrode.

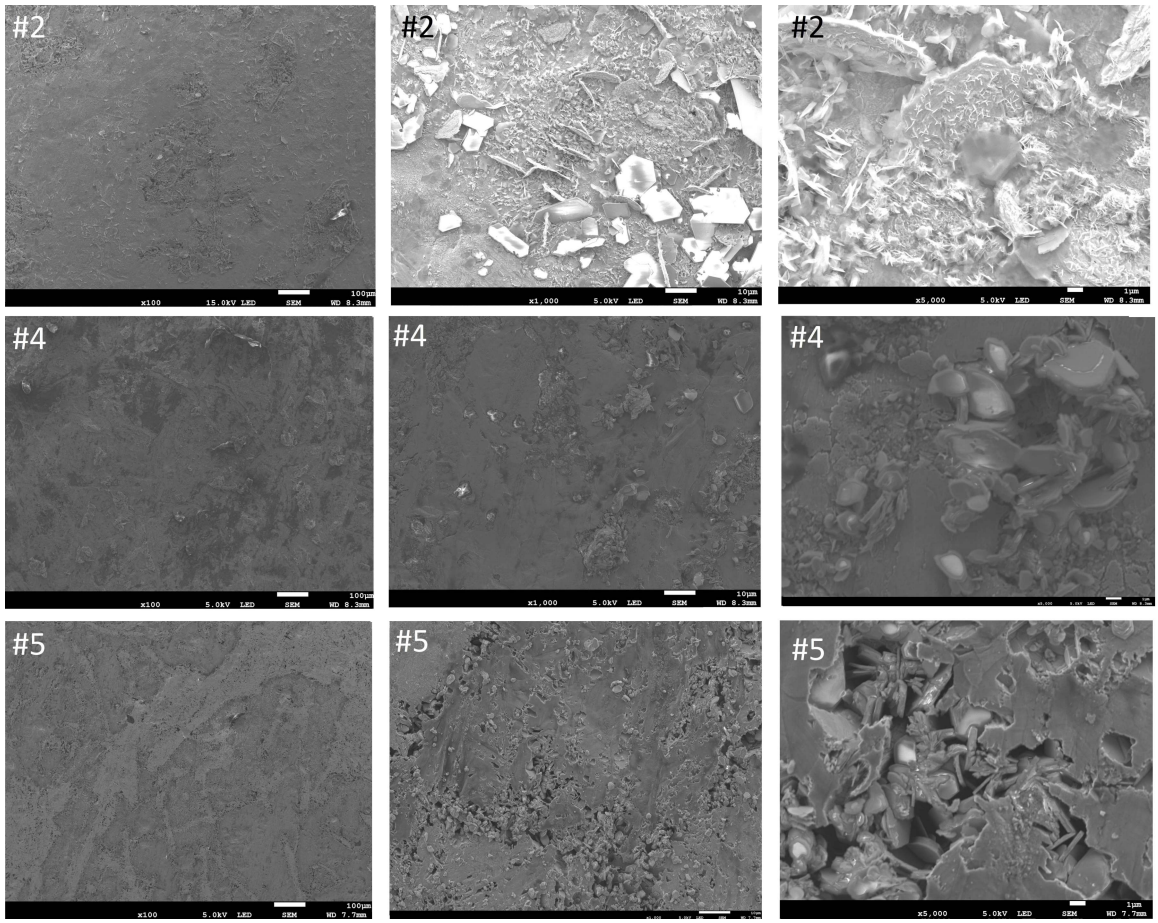

Figure 5.15: Images of zinc electrodes after cycling with electrolyte #2 (top row), electrolyte #4 (middle row), and electrolyte #5 (bottom row).

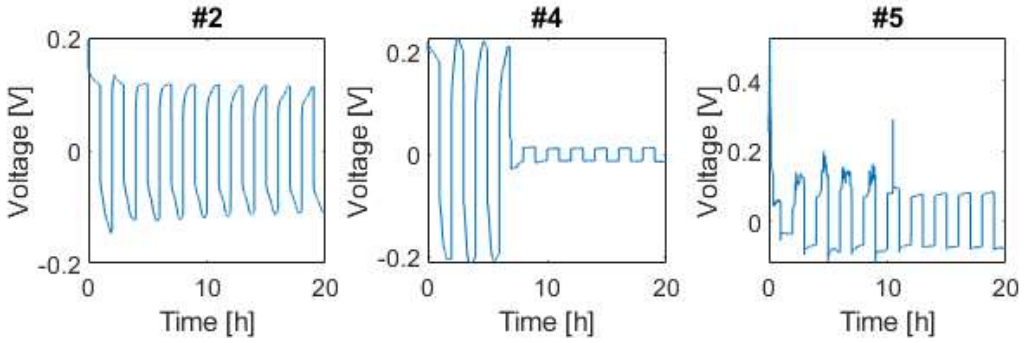

Figure 5.16: Cycling profiles from symmetric cells with the electrolytes #2, #4, and #5 used for SEM imaging, plating and stripping at 2mA/cm^2 for 1 hour each for 10 cycles.

In figure 5.17 the images of zinc deposition on copper with electrolytes #2, #4, and #5 are shown. In the images one can observe the grooves left from the fibers of the separator on the surface, and the bottom left image even shows some of the fibers of separator stuck to the surface. Zinc platelets ranging in sizes from less than 1 µm to more than 10 µm are again

observed with electrolyte #2. For electrolytes #4 and #5 a more narrow size distribution of the platelets is observed, with most platelets being between 1-10 µm. The cycling profiles for these cells are shown in figure 5.18.

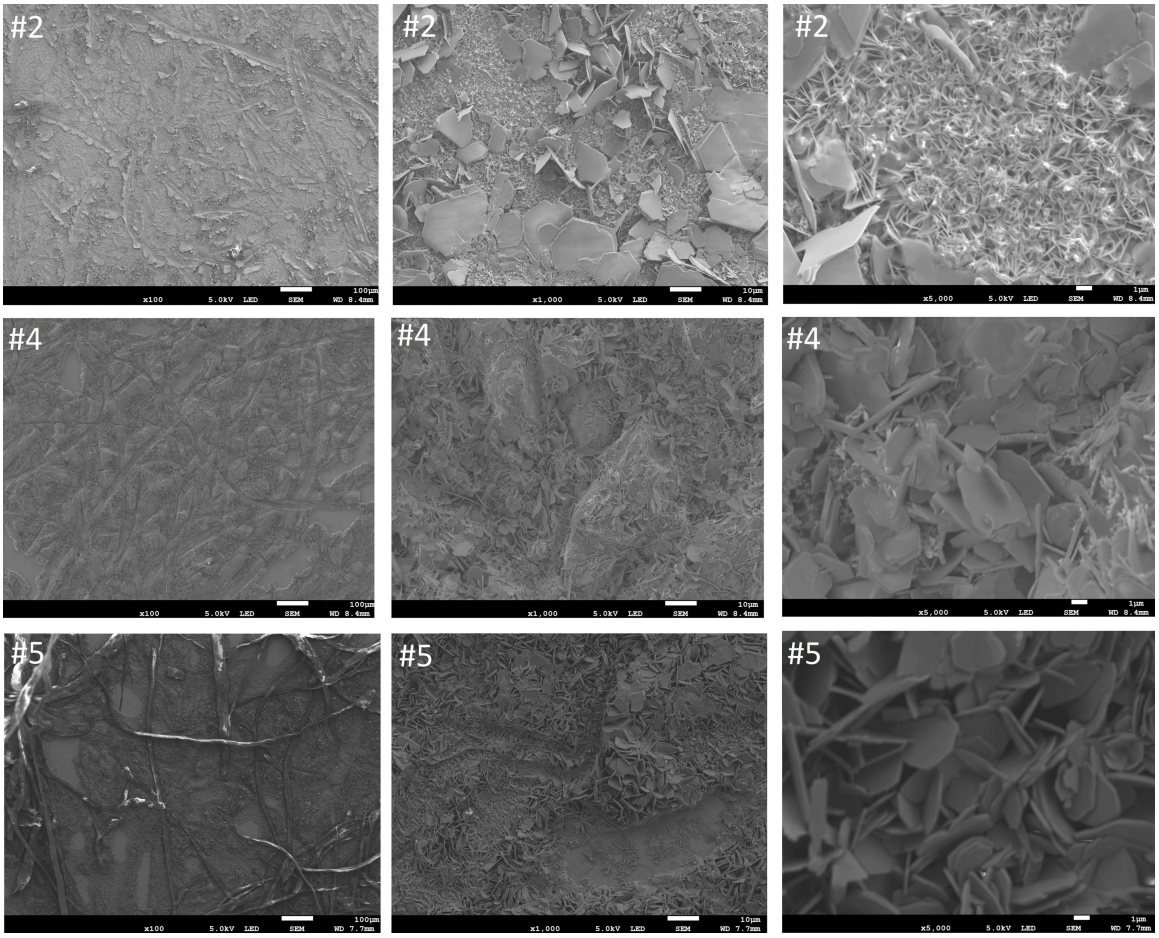

Figure 5.17: Images of copper electrodes after cycling with electrolyte #2 (top row), electrolyte #4 (middle row), and electrolyte #5 (bottom row).

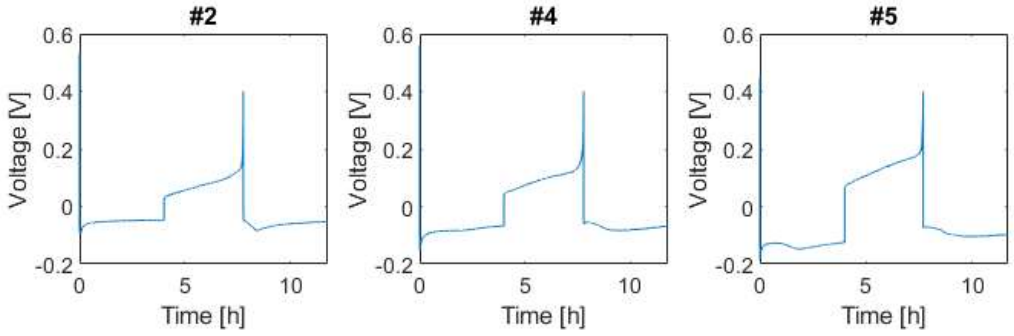

Figure 5.18: Cycling profiles from zinc/copper cells with electrolytes #2, #4, and #5 used for SEM imaging, plating at 0.5mAh/cm^2 for 4 hours then stripping until cutoff voltage of 0.4 V and then plate at 0.5 mAh/cm^2.

The images of zinc deposition onto the zinc surface with the electrolytes containing CMC and CNC are shown in figure 5.19. From the images for CMC containing electrolyte, two different morphologies of deposited zinc are observed, one looking smooth like the pristine zinc and one mossy like near the fibers of the separator. There is a high possibility that the smooth area is due to the removal of the mossy like growth when the separator was removed. Therefore, magnified images of the mossy like growth instead of the smooth surface are shown. The mossy growth containing hexagonal platelets where the largest ones are in the size range of 5-10 µm and the majority of the platelets are around 1 µm. For the CNC containing electrolyte, large smooth areas are observed together with some large structures. Magnifying these structures shows that there are no clearly hexagonal platelets. However, in the image with the highest magnification is it found that the structures are consisting of platelets smaller than 1 µm. The cycling profiles for these cells are shown in figure 5.20.

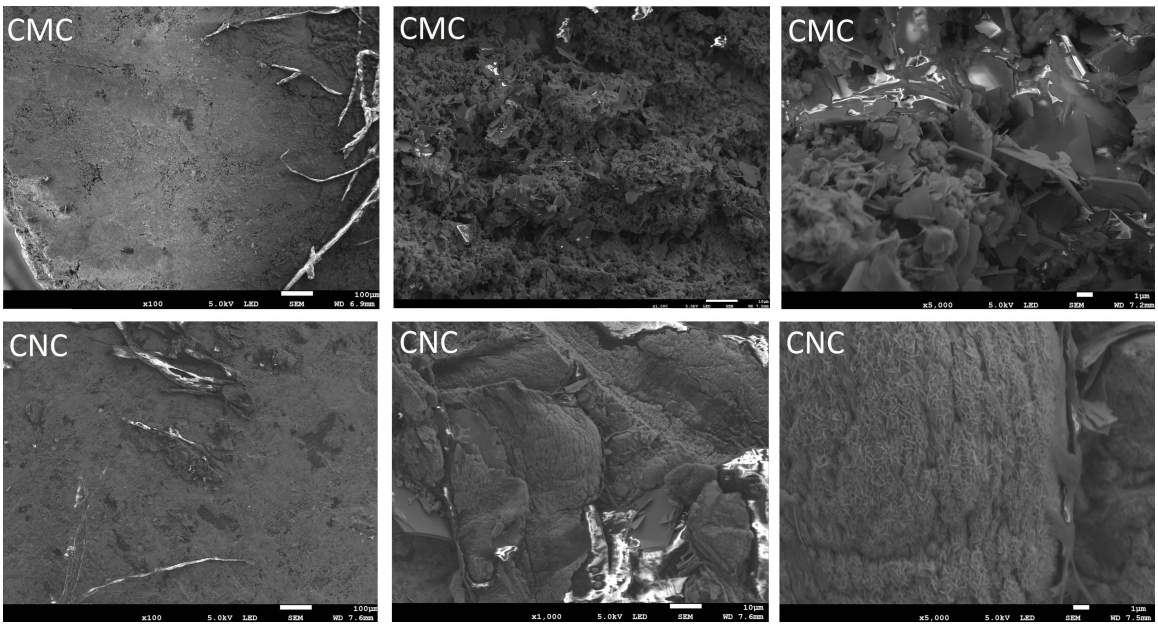

Figure 5.19: Images of zinc electrodes after cycling with electrolytes containing CMC (top row) and CNC (bottom row).

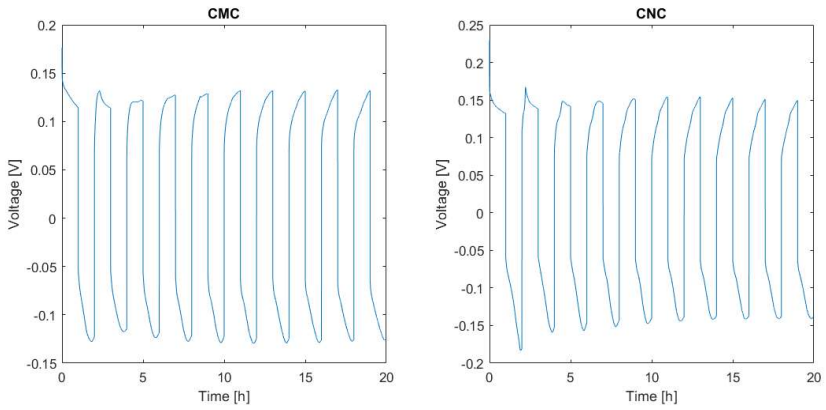

Figure 5.20: Cycling profiles from symmetric cells with electrolytes containing CMC and CNC that were used for SEM imaging, plating and stripping at 2mA/cm^2 for 1 hour each for 10 cycles.

In figure 5.21 images of zinc deposition onto the copper surface with the electrolytes containing CMC and CNC is shown. In the sample with electrolyte containing CMC, there seems to be fewer platelets smaller than 1 µm compared to what is found with electrolyte #2, (figure 5.17). It is also observed that in the middle image dendrite like structures are present. These structures are roughly 30-40 µm in diameter. In the sample with electrolyte containing CNC, larger platelets with a large amount of smaller ones in between are shown, which is quite similar to that of the sample with electrolyte #2. In the highest magnification of the CNC containing sample it shows small hexagonal platelets but in addition, irregularly shaped chunks. The cycling profiles for these cells are shown in figure 5.22.

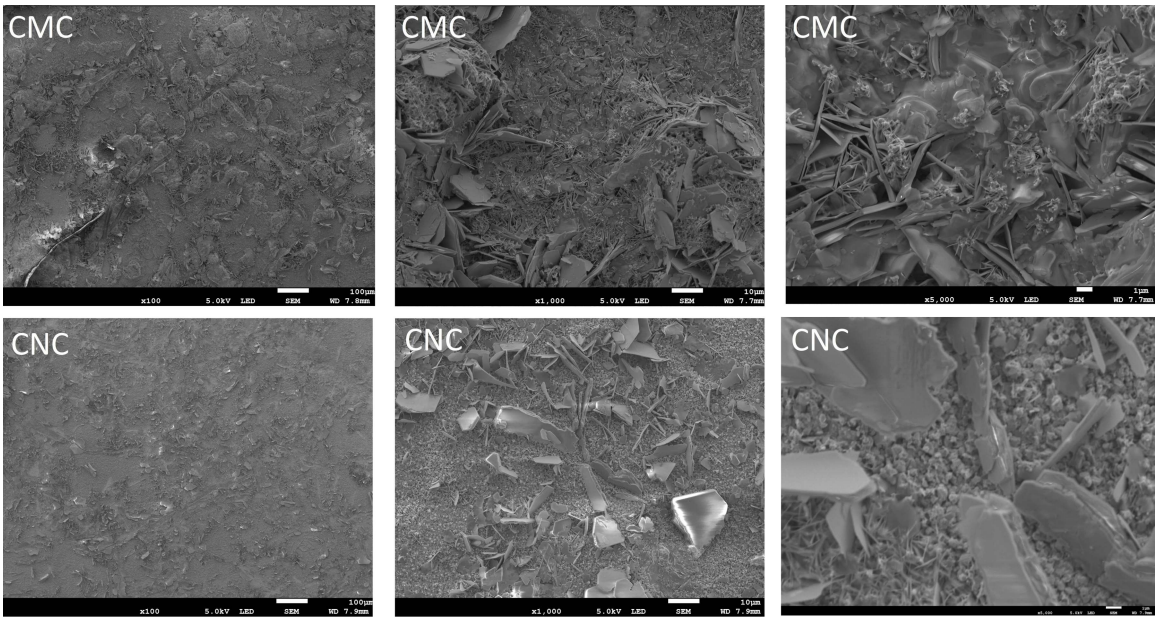

Figure 5.21: Images of copper electrodes after cycling with electrolytes containing CMC (top row) and CNC (bottom row).

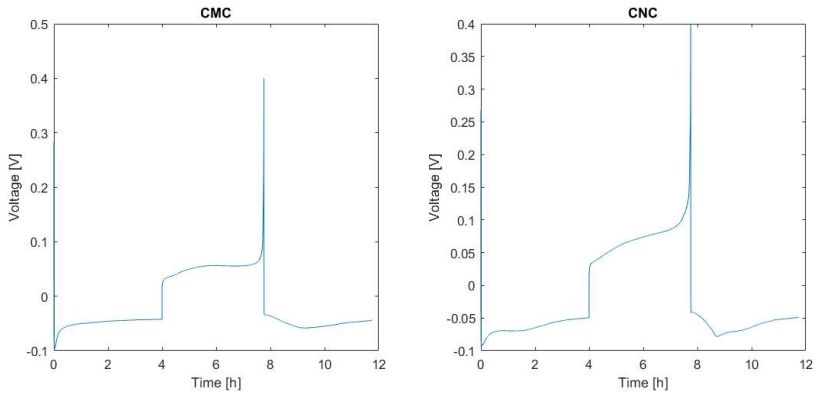

Figure 5.22: Cycling profiles from zinc/copper cells with electrolytes containing CMC and CNC that were used for SEM imaging, plating at 0.5mAh/cm^2 for 4 hours then stripping until cutoff voltage of 0.4 V and then plating at 0.5 mAh/cm^2 again.

To study short circuit induced by dendrite growth the middle separator was retrieved from short circuited cells and imaged by SEM. In figure 5.23 an example of a dendrite in the middle separator is shown. Figure 5.24 shows the electrolyte #4 sample and a structure that is roughly 80 µm across and covered by the typical hexagonal platelets. However, in the CMC containing electrolyte sample there are no large structures observed in the separator. Instead it seems like the platelets are growing in between and along the fibers of the separator.

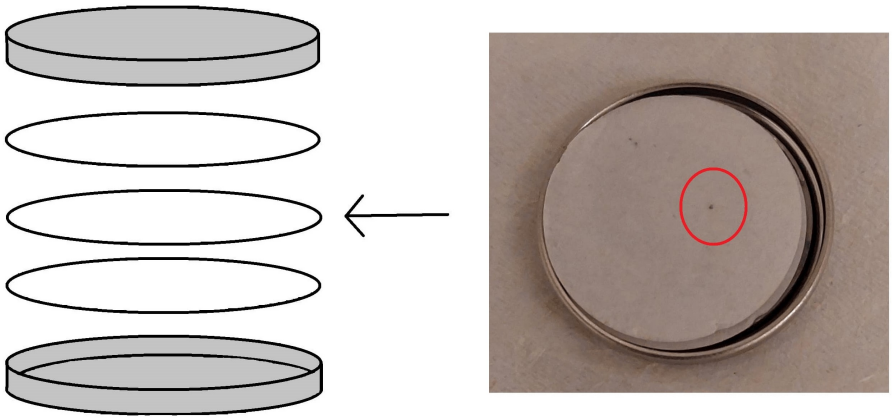

Figure 5.23: Image of a dendrite in the middle separator.

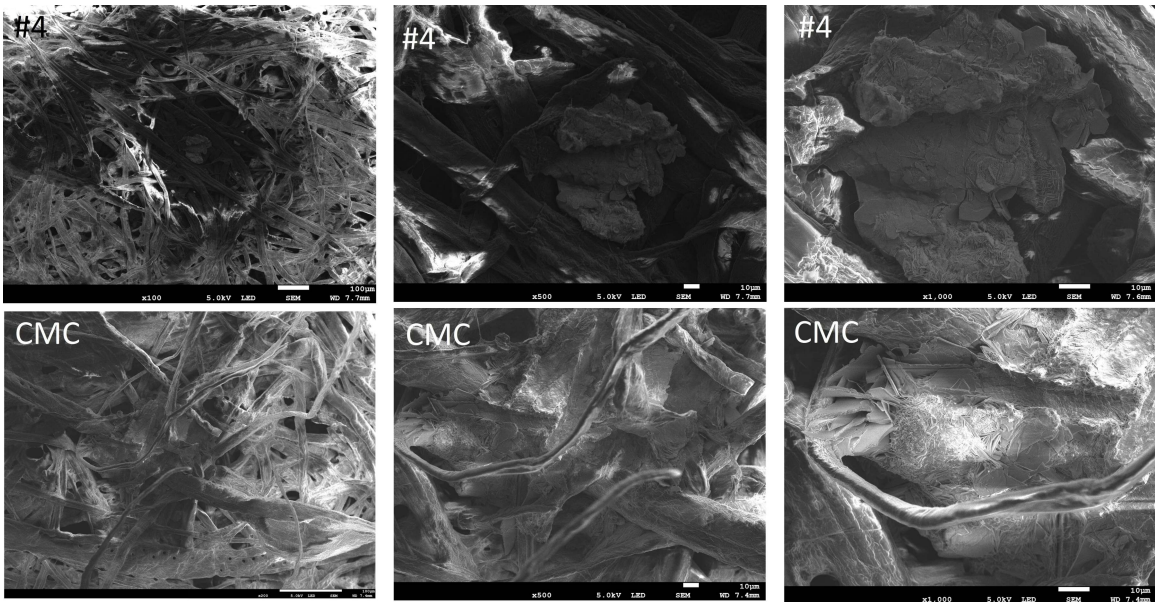

Figure 5.24: Images of dendrites from the middle separator of a short circuited symmetric cell with #4 electrolyte and electrolyte containing CMC.

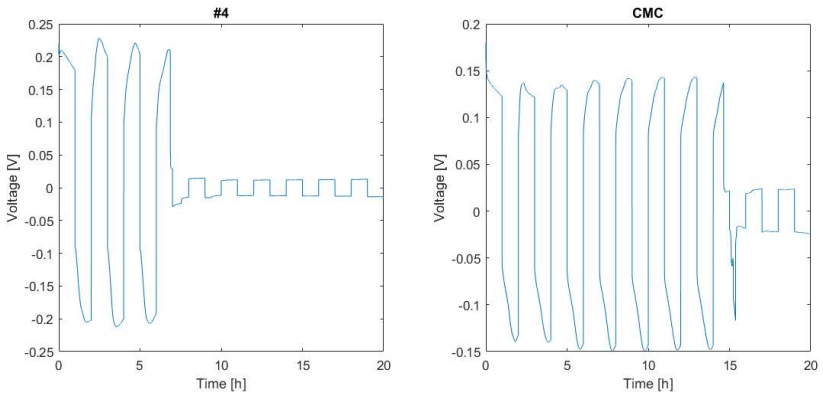

Figure 5.25: Cycling profiles from short circuited symmetric cells with electrolyte #4 and electrolyte containing CMC, plating and stripping at 2mA/cm^2 for 1 hour each for 10 cycles.

6

Conclusion and outlook

In this project the effects of the concentration of zinc sulfate heptahydrate in water electrolyte was studied. Both the physical properties and the effect on the electrochemical performance of coin cells were measured. In addition, the effect of the additives CNC and CMC was also studied. The results showed that among the electrolytes without additives electrolytes #2 and #3 showed the best performance in terms of both cycling stability and Coulombic efficiency. For the additives, the addition CNC improves the Coulombic efficiency while the addition of CMC improves the cycling stability of symmetric cells.

To study the morphology of zinc deposition onto the electrode an investigation with SEM was performed. The SEM images showed that the salt concentration as well as the addition of additives impacts the morphology of deposited zinc. The lower salt concentration of the samples with electrolyte #4 and #5 showed a narrower size range of the platelets on the copper surface compared to the sample with electrolyte #2. The addition of the additives showed a great impact on the morphology of the deposited zinc in the symmetric cells. The number of large platelets was greatly reduced and most of the zinc is deposited as small, roughly 1 µm, sized platelets.

Another aspect of interest is the different behaviors of dendrite growth through the separator, where in the sample with the electrolyte containing CMC the zinc dendrite grows along the fibers, while in the electrolyte #4 sample it seems to grow between the fibers. To confirm if this behavior is due to the different electrolytes or just a coincidence for these two cells, as well as determining if it has any effect on the stability of the cell could be of interest in further studies.

Based on the results of this project the additive CMC is suggested as a promising candidate for further investigation. It significantly improved the cycling stability of the cell while not decreasing the Coulombic efficiency. The aim of the further investigations could be to understand the mechanism behind the improvement. One could also further study the effect of CMC on the cycling stability of a full zinc-metal cell.

Bibliography

[1] Statista, "Projected global battery demand from 2020 to 2030, by application (in gigawatt hours)" Statista, `https://www.statista.com/statistics/1103218/global-battery-demand-forecast/` (Accessed May, 2022)

[2] M. S. Ziegler and J.E. Trancik, "Re-examining rates of lithium-ion battery technology improvement and cost decline", *Energy Environ. Sci.*,**14**, 1635-1651, (2021)

[3] K. Turcheniuk et al, "Ten years left to redesign lithium-ion batteries", *Nature*, **559**, 467-470, (2018)

[4] Y. Chen et al, "A review of lithium-ion battery safety concerns: The issues, strategies, and testing standards" *Journal of Energy Chemistry*, **59**, 83-99, (2021)

[5] W. Tahil. "The trouble with lithium", Meridian International Research, 2007

[6] R. F. Service, "Zinc aims to beat lithium batteries at storing energy", *Science*, **372**, 890-891, (2021)

[7] Y. Jin et al, "Stabilizing Zinc Anode Reactions by Polyethylene Oxide Polymer in Mild Aqueous Electrolytes", *Adv. Funct. Mater.*, **30**, 2003932, (2020)

[8] W. Du et al, "Challenges in the material and structural design of zinc anode towards high-performance aqueous zinc-ion batteries", *Energy Environ. Sci.*, **13**, 3330-3360, (2020)

[9] J. Zheng et al, " Reversible epitaxial electrodesposition of metals in battery anodes", *Science*, **366**, 645-648, (2019)

[10] D. Pletcher, "A first course in electrode processes", RSC publishing, 2nd edition, (2009)

[11] N. Nitta et al, "Li-ion battery materials: present and future", *Materials today*, **18**, 252-264, (2015)

[12] J. Murray, "Is the Nobel Prize-winning lithium-ion battery really having a positive impact on the environment?", NS Energy, `https://www.nsenergybusiness.com/features/lithium-ion-battery-environmental-impact/` (Accessed May 2022)

[13] N. Zhang et al, "Rechargeable aqueous zinc-manganese dioxide batteries with high energy and power densities", *Nat. Commun.*, **8**, 405, (2017)

[14] D. Kundu et al, "A high-capacity and long-life aqueous rechargeable zinc battery using a metal oxide intercalation cathode", *Nat. Energy*, **1**, 16119, (2016)

[15] P. He et al. "Layered VS_2 Nanosheet-Based Aqueous Zn Ion Battery Cathode", *Adv. Energy. Mater.*, **7**, 1601920, (2017)

[16] A. Naveed et al, "Highly Reversible and Rechargeable Safe Zn Batteries Based on a Triethyl Phosphate Electrolyte", *Angewandte Chemie*, **58**, 2760-2764, (2019)

[17] Z. Guo et al, "An Environmentally Friendly and Flexible Aqueous Zinc Battery Using an Organic Cathode", *Angewandte Chemie*, **57**, 11737-11741, (2018)

[18] Z. Cheng et al, "Toward Safe Lithium Metal Anode in Rechargeable Batteries: A Review", *Chem. Rev.*, **117**, 10403-10473, (2017)

[19] R. Boddula et al, "Electrolytes for Zn-Ion Batteries", in *Zinc batteries basics, developments, and applications*, Beverly, MA, USA, Scrivener publishing, 2020, ch 5, pp 51-71

[20] Y. Shang, D. Kundu "Understanding and Performance of the Zinc Anode Cycling in Aqueous Zinc-Ion Batteries and a Roadmap for the Future", *Batteries Supercaps*, **5**, e202100394, (2022)

[21] "Laboratory density and concentration meters", Anton Paar, `https://www.fourni-labo.fr/entreprise/doc/0855e45a64d1652abc6407745985884f2954356974.pdf`, (2020)

[22] M. Kerner, "Pure, hybrid and polymerized ionic liquid based electrolytes", Ph.D. dissertation, Physics, Chalmers, Gothenburg, (2017)

[23] B. D. Adams et al, "Accurate Determination of Coulombic Efficiency for Lithium Metal Anodes and Lithium Metal Batteries", *Adv. Energy. Mater.*, **8**, 1702097, (2018)

[24] X. Yu et al, "Role of Li-Ion Depletion on Electrode Surface: Underlying Mechanism for Electrodeposition Behavior of Lithium Metal Anode", *Adv. Energy. Mater.*, **10**, 2002390, (2020)

DEPARTMENT OF PHYSICS
CHALMERS UNIVERSITY OF TECHNOLOGY
Gothenburg, Sweden
www.chalmers.se

CHALMERS
UNIVERSITY OF TECHNOLOGY